

# Stall/Spin Flight Testing with a Subscale Aerobatic Aircraft

Adam M. Ragheb,\* Or D. Dantsker,† and Michael S. Selig‡

*University of Illinois at Urbana-Champaign, Department of Aerospace Engineering, Urbana, IL 61801*

The effects of configuration changes on the stall/spin characteristics of a single-engine subscale airplane are presented. A 35%-scale, 2.7-m (105-in) wingspan Extra 260 electric aircraft, the UIUC Aero Testbed, was used for this research. A series of flight tests were conducted with the instrumented aircraft, and over 20 different stall/spin maneuvers with varying control surface inputs, combinations, and deflections were studied. Select maneuvers were then tested with three different ventral fins, and the effects on the steady-state spin and recovery were analyzed. The data acquired by the onboard inertial measurement unit (IMU) showed which control inputs would produce a slower or more-easily recoverable stall/spin and which ventral fins were the most effective in improving the stall/spin and/or the recovery from the high bank and high yaw rates of the spin. It was observed that an increase in the motor power setting above the windmilling RPM of the propeller had an adverse effect on the spin recovery, and this adverse effect was worsened when the ailerons were deflected in an anti-spin manner. Additionally, it was observed that the installation of ventral fins removed the ability of the aircraft to spin with anti-spin deflected ailerons. For the testbed aircraft studied, a neutral-aileron spin mode occurred at approximately a pitch of  $-55$  deg, a vertical velocity of  $-15$  m/s, a roll rate of 235 deg/s, and a spin parameter magnitude of 0.20. The addition of pro-spin ailerons on average lowered the nose 5 deg, increased the vertical velocity in the negative direction by 66%, increased the roll rate by 50%, and halved the magnitude of the spin parameter, while the addition of anti-spin ailerons on average raised the nose 10 deg, reduced the roll rate by 20%, had no significant effect on the vertical velocity, and increased the magnitude of the spin parameter by 50%. These data will be used to investigate and model the complex aerodynamics experienced by the airplane in a stall/spin situation, and the results of the process of modeling the aerodynamics should be useful in the preliminary design stages of a general aviation aircraft to provide a better design-for-spin.

## Nomenclature

$b$	= wing span
$c$	= wing chord
$\bar{c}$	= wing mean aerodynamic chord
$g$	= gravitational constant
$I_{xx}, I_{yy}, I_{zz}$	= roll, pitch, and yaw mass moments of inertia
$(I_{xx} - I_{yy})/mb^2$	= inertia yawing moment parameter ( <i>IYMP</i> )
$(I_{yy} - I_{zz})/mb^2$	= inertia rolling moment parameter ( <i>IRMP</i> )
$(I_{zz} - I_{xx})/mb^2$	= inertia pitching moment parameter ( <i>IPMP</i> )
$m$	= airplane mass
$p, q, r$	= roll, pitch, and yaw rates
$R_s$	= spin radius
$RC$	= radio controlled
$Re$	= Reynolds number based on mean aerodynamic chord ( $V\bar{c}/\nu$ )
$S$	= reference area
$V$	= inertial speed
$x, y, z$	= position of the airplane trajectory
$\alpha$	= angle of attack (referenced to fuselage)
$\beta$	= sideslip angle
$\delta_a, \delta_e, \delta_r$	= aileron, elevator, and rudder deflections

\*PhD Candidate, Department of Aerospace Engineering, 104 S. Wright St., AIAA Student Member, aragheb@illinois.edu.

†Graduate Student, Department of Aerospace Engineering, 104 S. Wright St., AIAA Student Member, dantske1@illinois.edu.

‡Associate Professor, Department of Aerospace Engineering, 104 S. Wright St., AIAA Senior Member, m-selig@illinois.edu.

$\lambda$	= taper ratio
$\mu$	= airplane relative density [ $W/(\rho Sgb)$ ]
$\nu$	= kinematic viscosity
$\rho$	= air density
$\sigma_\theta$	= standard deviation of pitch angle
$\phi, \theta, \psi$	= roll, pitch, and heading angles
$\omega$	= spin coefficient ( $\Omega b/2V$ )
$\Omega$	= angular velocity about axis of spin

#### Subscripts

$H$	= property of the horizontal stabilizer
$T$	= property of the vertical stabilizer
$W$	= property of the wing
$Wr$	= property of the wing root
$Wt$	= property of the wing tip

## I. Introduction

There has been an interest in studying aircraft spin since the biplane era of the early 1930s<sup>1</sup> when the NACA staff first dropped dynamically-scaled models from the top of a 105-ft balloon hangar in order to study how to improve the spin characteristics of the NB-1 seaplane trainer and the O2-E observation airplane.<sup>2</sup> The free-drop method<sup>1</sup> yielded too short of a timeframe for conducting satisfactory tests, and by 1932 researchers in England had constructed the first operational vertical spin tunnel with a 12-ft diameter<sup>3</sup> circular test section. It has been said “stall/spin problems represent one of the last technical frontiers in the aviation field and have significant impact on the general-aviation (GA) industry.”<sup>4</sup> Stall/spin is a difficult problem due to the high angles of attack<sup>5-7</sup> involved and the associated highly-separated flow. In addition, any extrapolation from spin tunnel or radio-controlled (RC) model tests is difficult because of critical Reynolds number effects.<sup>8,9</sup>

The study of spin among GA-sized aircraft is an important topic. Accidents in which stall/spin are cited account for about 7% of total pilot-related single-engine accidents yet these accidents represent a staggering 65–70% of the total fatalities.<sup>10</sup> The only deadlier causal factor cited in accidents is weather, which is cited in only 5–6% of total pilot-related single-engine accidents but is a factor in 65–75% of the fatalities. The most common type of pilot-related single-engine accidents is listed as landing accidents. Landing accidents account for approximately 45% of pilot-related accidents, but they represent only 1–2% of the total amount of fatalities. For purposes of clarity, multiple causal factors are often cited in aircraft accidents.<sup>10</sup>

Research attention to stall/spin increased in 1970 with the publishing of AAS-72<sup>11</sup> by the National Transportation Safety Board (NTSB)<sup>12</sup> which observed that, despite safety improvements, stall-related accidents were still the largest share of GA flying accidents. In fatal accidents where stall or mush were the first or second accident type, the fatal accident rate per 100,000 flight hours showed a strong relationship to the airplane model, with the Cessna 182 exhibiting a low accident rate of 0.12 and the Globee GC-1 a high accident rate of 3.05,<sup>12</sup> illustrating that some airplanes had better design-for-spin than others.<sup>11</sup>

The seminal paper on this topic is Tail-Design Requirements for Satisfactory Spin Recovery.<sup>13</sup> In this paper, a tail damping power factor ( $TDPF$ ) was proposed. Bowman<sup>14</sup> expanded upon the work of Ref. 13 in 1971 and highlighted the different factors that contribute to aircraft spin. A number of significant factors were identified, and for GA aircraft, the three primary factors were listed as the mass distribution, relative density, and tail configuration. Additional factors were listed as the trailing-edge flaps, landing gear, and length of the tail. Factors identified as being secondary to the spin characteristics included the center of gravity (CG) location, the wing fuel tanks, the aircraft power setting, and the wing position.<sup>14</sup> In short, the tail geometry was discovered to not be the sole factor ensuring satisfactory spin recovery for an aircraft.

NASA began to “back away” from using the  $TDPF$  as the sole criterion<sup>15-17</sup> with the loss of a T-tail test aircraft with a  $TDPF > 800 \times 10^6$ , a value well above the threshold for good spin recovery characteristics<sup>17</sup> of  $TDPF > 600 \times 10^6$  and airplane relative density  $\mu \leq 20$  as suggested by Ref. 13. When compared with earlier versions of the test aircraft, the aircraft that was lost had an extended nose section with strakes.<sup>17</sup> According to McCormick,<sup>18</sup> to

have reasonable spin recovery characteristics, the pitch and roll moments of inertia of an aircraft must exhibit a large difference.

In 1974, NASA and Piper assessed the use of RC aircraft for stall/spin research, and in 1975, Beech teamed with NASA to test the accuracy of RC model tests for the YT-34C airplane and found that when the same spin mode developed, the RC and full-scale aircraft results agreed quite well.<sup>19</sup> There were a number of cases, however, when the RC and full-scale airplanes did not develop the same spin modes, an occurrence that was attributed to Reynolds number effects.<sup>19</sup> Despite this issue, Beech used spin tunnel and RC models in its Model 77 “Skipper” program. The 20%-scale model used by Beech was the first instance of an instrumented RC model being used for the development of a GA aircraft. The spin angle of attack for the models was around 15 deg less than that of the aircraft, and because of this, it was concluded that models could only be used for trends and not for quantitative results because of Reynolds number effects.<sup>19</sup>

In 1977 a French paper by Beaurain<sup>20</sup> was translated, noting that an aft fuselage with a flat top and a round bottom was the best for spin recovery. Beaurain also studied the width of the aft fuselage but found it to be much less significant than the shape. This round-bottom and flat-top fuselage is the opposite of what many GA aircraft use, with the current flat-bottom and round-top fuselage providing better lifting and cargo-carrying capabilities. Bihrlé and Bowman<sup>21</sup> conducted studies that included changes to the aft fuselage shape and converged on the same results as Beaurain.

The effectiveness of antispin fillets and ventral fins has proven itself on the Pilatus PC-21 advanced-turboprop trainer. The development program for the PC-21 worked with Bihrlé Applied Research, conducting spin testing at the Large Amplitude Multi-Purposed (LAMP) 10-ft diameter spin tunnel in Neuberg an der Donau.<sup>22</sup> Bihrlé Applied Research was founded by the same William Bihrlé who commenced his spin work at NASA Langley, and the rotary balance data from the PC-21 was used to determine that stabilizer “strakes”<sup>22</sup> (i.e., antispin fillets) produced a nose-down pitching moment that stabilized the spin. In this case, however, Pilatus had the goal of making a previously unspinnable airplane spin in a stable and recoverable mode. Through extensive testing, Pilatus was able to achieve the goal of generating a stable spin model by reducing the size of the ventral fin, changing its shape to a ventral “bump,” and sweeping the vertical tail back. To create a stable and more-recoverable spin mode, horizontal stabilizer strakes were added to stabilize the spin in a more nose-down, and thus more recoverable, spin mode.<sup>22</sup>

In regards to the Cessna 162 SkyCatcher, the inability of early prototypes to recover acceptably from an intentional spin was solved by increasing the size and reducing the sweep of the vertical tail,<sup>23</sup> extending the rudder further down, and adding a large ventral fin.<sup>24</sup> A dorsal fin was also tested during an interim configuration, but it was not included on the production aircraft.<sup>23</sup>

This paper will discuss the flight vehicle setup and the flight tests performed in order to characterize a number of spin configurations. The different combinations of control surface deflections, motor power setting, and upright versus inverted flight used in the spins are covered, and the resulting spins are presented and characterized. A specific emphasis is placed on the changes in the spin characteristics due to changes in the aircraft configuration. Three ventral fins are tested, motivated by the addition of a ventral fin to the production SkyCatcher aircraft, and their effects on the spins and recoveries are discussed.

## II. Flight Vehicle and Instrumentation Experimental Setup

In this work, the UIUC Aero Testbed, an RC testbed aircraft with an onboard instrumentation system, was flown into over 250 spins, comprising a number of different control deflection combinations and ventral fin additions. Parameters that were varied include: direction of spin, magnitude of the control deflections, combination of control surface deflections, whether the spin was from upright or inverted flight, and motor power setting. Spins were verified to exhibit similar performance throughout the testing program, and the majority of spin configurations achieved a near-steady state motion. The instrumentation provided time histories of the trajectory, velocity, acceleration, angular rates, and airspeed. From these data, the spin and recovery characteristics of the testbed aircraft were determined. Additionally, ventral fins of three different geometries were installed on the airplane, and their effects on the spin and recovery characteristics were recorded.

The UIUC Aero Testbed aircraft used in the testing was developed<sup>25</sup> from a commercially available almost ready-to-fly (ARF) 35%-scale Extra 260 produced by Horizon Hobby’s Hangar 9 division.<sup>26</sup> Table 1 lists the physical properties of the airplane. The airplane had a wingspan of 105 in (266.7 cm) and a weight of 37.51 lb (17.01 kg). A photograph of the Extra 260 is shown in Fig. 1. Based on the mean aerodynamic chord, the airplane has a nominal cruise Reynolds number range of  $7\text{--}9 \times 10^5$  at a  $C_L$  of 0.3–0.5. When in a spin condition, the wing-tip Reynolds number was in the vicinity of  $5 \times 10^5$ . The tapered wing had a 10.5%-thick symmetric airfoil, a taper ratio of 0.45,

and an aspect ratio of 5.50. The horizontal and vertical tail surfaces consisted of symmetric airfoils with a  $t/c$  of 11%, and both wing and horizontal tail had zero dihedral and zero incidence. In order to reduce vibrations and avoid inflight changes to the weight and center of gravity (CG), the aircraft was powered by a Hacker A150-8 electric motor fitted with a Mejzlik 27x12TH propeller. To counteract the left turning tendencies caused by the propeller wake swirl, the motor was angled 2.5 deg to the right. There was zero down thrust. A 14-cell, 51.8V, 10,000-mAh lithium polymer (LiPo) battery provided a power source for the motor. This power source provided approximately 8 min of flight time when performing spins and as much as 12 min of flight time when performing primarily steady cruise flight with some gentle climbs and glides.

**Table 1. Physical Properties of the 35%-Scale Extra 260 Aircraft**

Aircraft		
Length	245.9 cm	(96.8 in)
Nose/Tail length ratio	0.44	
Mass / Weight	17.01 kg	(37.51 lb)
CG location ( $\% \bar{c}$ )	35.2% $\bar{c}$	
Roll moment of inertia ( $I_{xx}$ )	1.53 kg-m <sup>2</sup>	(1.13 slug-ft <sup>2</sup> )
Pitch moment of inertia ( $I_{yy}$ )	4.86 kg-m <sup>2</sup>	(3.58 slug-ft <sup>2</sup> )
Yaw moment of inertia ( $I_{zz}$ )	6.06 kg-m <sup>2</sup>	(4.47 slug-ft <sup>2</sup> )
Wing		
Span ( $b$ )	266.7 cm	(105.0 in)
Area ( $S_W$ )	13,118.2 cm <sup>2</sup>	(2033.3 in <sup>2</sup> )
Root chord ( $c_{Wr}$ )	66.7 cm	(26.3 in)
Tip chord ( $c_{Wt}$ )	30.2 cm	(11.9 in)
Taper ratio ( $\lambda$ )	0.45	
Mean aerodynamic chord ( $\bar{c}$ )	50.7 cm	(20.0 in)
Airfoil $t/c$	10.5%	
Airfoil	Symmetrical	
Aspect ratio ( $\mathcal{A}$ )	5.50	
Incidence angle	0.0 deg	
Dihedral	0.0 deg	
Sweep	< 1 deg	
Vertical Stabilizer		
Area ( $S_V$ )	1379.4 cm <sup>2</sup>	(213.8 in <sup>2</sup> )
Rudder Area	990.3 cm <sup>2</sup>	(153.5 in <sup>2</sup> )
Airfoil $t/c$	11%	
Airfoil	Symmetrical	
Horizontal Stabilizer		
Area ( $S_H$ )	2895.0 cm <sup>2</sup>	(448.7 in <sup>2</sup> )
Elevator area	1315.0 cm <sup>2</sup>	(203.8 in <sup>2</sup> )
Root chord ( $c_{Hr}$ )	36.6 cm	(14.4 in)
Tip chord ( $c_{Ht}$ )	20.3 cm	(8.0 in)
Airfoil $t/c$	11.0%	
Airfoil	Symmetrical	
Aspect ratio ( $\mathcal{A}$ )	4.90	
Incidence angle	0.0 deg	
Dihedral	0.0 deg	

A total of three different flat-plate ventral fins were tested on the airplane to determine which tail and aft fuselage geometries most significantly affect the spin condition, and Fig. 2(a) provides a photograph of the ventral fin installation on the testbed aircraft. The fins were affixed to the airframe with four bolts that threaded into an equal number of blind nuts affixed to the internal structure of the aircraft tail. The aforementioned attaching method was devised in



Figure 1. A photograph of the 35%-scale Extra 260 UIUC AeroTestbed aircraft.

order to allow for rapid installation and removal of the ventral fins at the field. The fins were constructed of 1/8-in birch plywood that was glued and buttressed with 1/2-in basswood triangle stock. Lightening holes were made to Fins 2 and 3 in order to keep the weight similar to that of Fin 1. Covering was then applied to maintain the flat-plate surface. The properties of the three ventral fins are presented in Table 2, and a drawing of the three fins is presented in Fig. 2(b). The row entitled “Area under h-stab” refers to the area of the fin that is located beneath the horizontal stabilizer, as opposed to the area of the ventral fin that extends forward of the leading edge of the horizontal stabilizer. The inclusion of this measurement was prompted by the geometries used in calculating the  $TDPF$ .<sup>13</sup>

During a test flight, the trajectory and orientation of the aircraft was recorded using an Xsens MTi-G inertial measurement unit (IMU). The Xsens MTi-G contains a GPS-aided MEMS-based IMU. For trajectory tracking, the GPS signal is augmented by barometric pressure and inertial measurements to produce 3D location and velocity data superior to that of a standalone GPS receiver. The airplane is fitted with a single GPS antenna located atop the fuselage directly aft of the canopy (see Fig. 1). The IMU, located near the aircraft CG, is programmed to automatically correct the GPS location data based on the offset between the IMU and the GPS antenna. The data from the onboard Attitude and Heading Reference System (AHRS) and navigation processor undergo onboard real-time digital signal processing to produce filtered data based on the linking of the GPS, inertial, and barometric pressure recording devices.<sup>27</sup> Control surface positions, motor power settings, and motor RPM values are recorded by an Eagle Tree recording system.<sup>28</sup> A photograph of the electronics system is shown in Fig. 3.

While the velocity and orientation information is recorded in the Earth-reference frame, the acceleration and angular rate data are recorded in the body-fixed reference frame of the aircraft. When the motor power setting is

Table 2. Physical Properties of the Ventral Fins

	Fin 1		Fin 2		Fin 3	
Height	6.4 cm	(2.5 in)	6.4 cm	(2.5 in)	8.9 cm	(3.5 in)
Length	24.8 cm	(9.75 in)	36.6 cm	(14.4 in)	24.8 cm	(9.75 in)
Area	137.4 cm <sup>2</sup>	(21.3 in <sup>2</sup> )	200.0 cm <sup>2</sup>	(31.0 in <sup>2</sup> )	180.6 cm <sup>2</sup>	(28.0 in <sup>2</sup> )
Area under h-stab	137.4 cm <sup>2</sup>	(21.3 in <sup>2</sup> )	157.3 cm <sup>2</sup>	(24.4 in <sup>2</sup> )	180.6 cm <sup>2</sup>	(28.0 in <sup>2</sup> )
Weight	85.1 g	(3.0 oz)	93.6 g	(3.3 oz)	90.7 g	(3.2 oz)

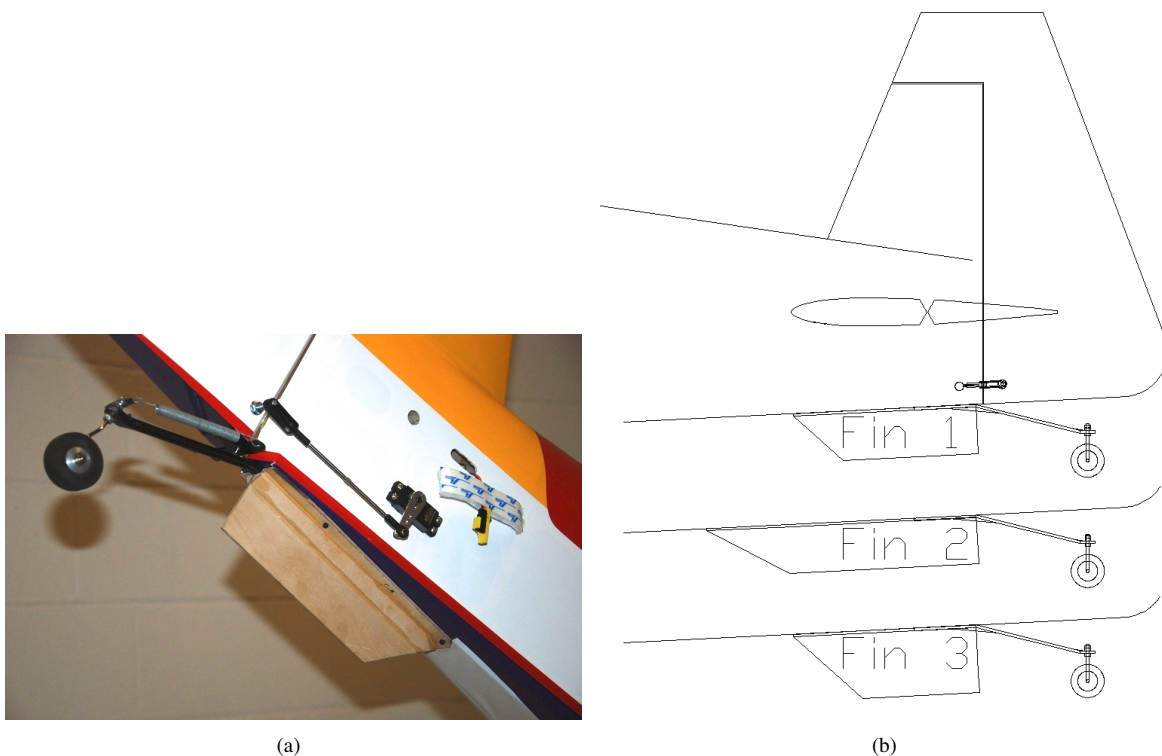


**Figure 2. Depiction of the ventral fin installation by (a) a photograph of Fin 1 installed on the testbed aircraft and (b) a CAD drawing of the three fins.**

increased, the electric motor induces a change in the local magnetic field and thus creates a change in the heading observed by the IMU but not in the angular rates and GPS position. The proximity of the IMU to the batteries is necessary in order to locate the IMU as close as possible to the CG of the airplane, and this location was chosen because it would give the highest accuracy measurements of the angular rates, accelerations, and orientation of the aircraft. The consequence of this location is that the measured heading  $\psi$  will slew when power is applied. All of the spins were conducted at a constant motor power setting, and the majority of the spins were conducted at a zero power setting.

The specified maximum operating altitude of the XSens MTi-G IMU is 18 km, the maximum operating velocity is 600 m/s, and the GPS resolution is 2.0 or 2.5 m<sup>27</sup> depending on satellite coverage. The dynamic accuracy of the IMU is 1-deg root mean squared (RMS) in roll and pitch and 2-deg RMS in heading. The GPS data is updated at a rate of 4 Hz, and the position and velocity is updated at 120 Hz.<sup>27</sup> The orientation and position of the IMU is estimated by means of an extended Kalman filter termed the Xsens Kalman Filter 6DOF GPS (XKF-6G). Since the GPS updates at 4 Hz while the inertial sensors update at 120 Hz, the data from the inertial sensors are integrated in order to predict the position and orientation. Due to small errors in the measurements, the orientation estimates will experience a growing error of approximately 3–4 deg/min. This growing error, or drift, is corrected using the GPS receiver. The result is a system that is able to estimate the position at a rapid update rate with minimal latency relative to a GPS-only system (like the Eagle Tree). As a result, small, rapid displacements may be quantified.<sup>27</sup> Altitude estimates from the GPS are supplemented by the internal barometer due to the inherent low accuracy of the GPS in sensing vertical position. The barometer is used only to sense the change in altitude because the pressure varies from day-to-day.<sup>27</sup>

The aircraft is also instrumented with a pitot-static airspeed measuring system. The pitot probe geometry allows it to record accurate dynamic pressures at flow angles up to 20 deg. Due to the high angles of attack experienced in a spin, the static pressure is not measured on the pitot probe; it is measured from inside the aircraft. The pitot probe and static tube are connected to a miniature amplified output pressure sensor. The device is 0.62 × 0.50 in and is temperature compensated, producing a linear output to the measured pressure. The 20cmH2O-D1-4V-MINI pressure sensor has an operating pressure range of –0.2 to 20 cm water and is temperature compensated between 5 and 50 deg C.<sup>29</sup>

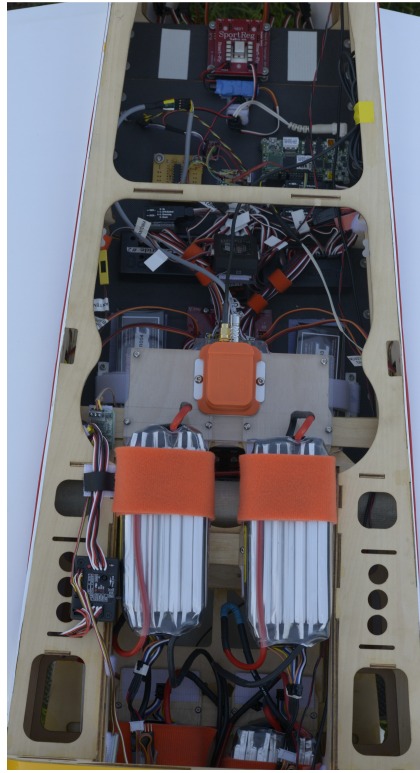


**Figure 3. A photograph of the instrumentation system on the testbed aircraft.**

The IMU and pitot probe data were transferred through a Paparazzi UAV autopilot board and recorded at 5 Hz on a Gumstix microcomputer running the Linux Ubuntu operating system. This system operated independently of the other two electrical systems on the aircraft. The second electrical system ran the RC receiver, servos, and the Eagle Tree recording device. The third and final electrical system powered the electric motor and was described in detail earlier in this section.

The airplane was flight tested at a CG location of 35.2%  $\bar{c}$ . The maximum control deflections at both the low and high deflection rates are presented in Table 3. In this context, “low rate” and “high rate” refer to the low and high deflection angles, respectively, and will henceforth be referred to as such.

### III. Spin Parameters

The standard nondimensional value adopted for describing spins is the spin parameter as given by<sup>7,30–32</sup>

$$\omega = \frac{\Omega b}{2V} \quad (1)$$

where  $b/2$  is the wing semispan,  $\Omega$  is the angular velocity about the spin axis in rad/s, and  $V$  is the freestream velocity. The spin parameter (Eq. 1) is a measure of the flatness of a spin. Low values of  $\omega$  correspond to a steep spin, while  $\omega$  values above 0.9 correspond to a flat spin mode.<sup>7</sup> This quantity is, by definition, positive for a nose-right spin.

**Table 3. Maximum Control Surface Deflection Angles**

Control Surface	Low Deflection (deg)	High Deflection (deg)
Rudder ( $\delta_r$ )	$\pm 29$	$\pm 40$
Elevator ( $\delta_e$ )	$\pm 14$	$\pm 46$
Ailerons ( $\delta_a$ )	$\pm 22$	$\pm 34$

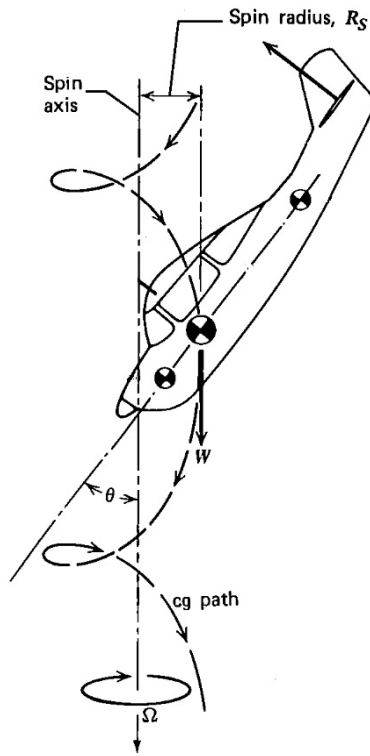


Figure 4. An illustration of the spin parameter variables (taken from Ref. 18).

Because the pitot probe is located on the left wing tip while the IMU is located near the CG of the airplane and the airplane spins about a helix with a non-zero radius (i.e., airplane CG does not pass through spin axis), the as-recorded velocity must be corrected. This velocity correction involves the geometric distance from the airplane centerline and the spin radius; the latter is calculated by<sup>18</sup>

$$R_s = \frac{g}{\Omega^2 \tan \theta} \quad (2)$$

where  $\theta$  is the pitch angle of the airplane and  $g$  is the gravitational acceleration. Figure 4 depicts the spin parameter variables.<sup>18</sup>

One of the three primary spin factors identified for general aviation aircraft is the mass distribution of the airplane;<sup>14</sup> the other two are the relative density  $\mu$  and the tail configuration. The mass distribution of an airplane is described through the nondimensional inertia yawing moment parameter given by<sup>14</sup>

$$IYMP = \frac{I_{xx} - I_{yy}}{mb^2} \quad (3)$$

where  $I_{xx}$  and  $I_{yy}$  are the roll and pitch moments of inertia, respectively. An aircraft that has its weight primarily distributed along the wing would have a positive  $IYMP$ , indicating that the roll moment of inertia  $I_{xx}$  is greater than the pitch moment of inertia  $I_{yy}$ . These aircraft are referred to as having a “wing-heavy loading”<sup>14</sup> and typically would have wing-tip tanks or twin wing-mounted engines. An aircraft that has the majority of the weight of the aircraft distributed longitudinally, and consequently has a pitch moment of inertia that is greater than the roll moment of inertia, would have a negative  $IYMP$ , or “fuselage-heavy loading.” Aircraft that have a fuselage-heavy loading would have their engines, fuel, cargo, and passengers located all in the fuselage. Single-engine general-aviation aircraft, the focus of this study, typically have a  $I_{yy}$  value that is close to  $I_{xx}$ . When  $I_{yy}$  and  $I_{xx}$  are close to the same value, the difference is near zero, and this loading case is consequently referred to as the “zero-loading case.” The zero loading case is typically defined as  $|IYMP| \leq 50 \times 10^{-4}$ . The AeroTestbed aircraft has an  $IYMP = -0.073$ , placing it within the boundaries of the “fuselage-heavy loading” case.

The relative density  $\mu$ , the second of the three primary factors identified by Bowman,<sup>14</sup> is the one spin factor that designers are least able to change. The relative density of an aircraft is defined by<sup>33</sup>

$$\mu = \frac{W/S}{\rho gb} \quad (4)$$

where  $S$  is the wing reference area and  $\rho$  is the air density. Because of the wing surface area parameter in Eq. 4, the airplane relative density is a form of a measure of wing loading. It was observed that an increase in  $\mu$  for the most part resulted in flatter spins, greater vertical velocities, more outward sideslip, and slower recoveries.<sup>33</sup> As an airplane development program progresses through the lifetime of the original design, the gross weight may be increased by means of additional fuel capacity, a larger and more-powerful engine, or a strengthened landing gear, among others. The increase in gross weight may significantly change  $\mu$  to the point where the aircraft may require an increase in the deflection or size of the rudder to maintain the original spin recovery characteristics. Variations of  $\mu$  due to different loadings of fuel, cargo, and passengers may be assumed to not appreciably change the value of  $\mu$ .<sup>14</sup> The value for the 35%-scale Extra 260 as tested in this research is  $\mu = 4.00$  for standard sea-level conditions.

#### IV. Results and Discussion

Results from a total of 24 different spins are hereby presented. Due to the large number of spin configuration variables, a rigidly-defined naming convention was constructed. For each spin, the rudder, elevator, and aileron deflections and directions, the motor power setting, and the installed ventral fin (if any) must be defined. The motor power setting is customarily called the throttle setting, and will be referred to as the latter. The construction of the naming convention allows for all of the information about the spin configuration to be conveyed to the reader with a string of letters, numbers, and dashes. The naming convention is organized into four sections, each of which is separated by a dash. The first section describes the throttle, rudder, elevator, and aileron settings in the conventional “TREA” order. Three possible throttle settings exist, “T0”, “T1”, and “T2”, and the approximate RPM values for each of these three settings are summarized in Table 4. Two settings for the rudder and elevator exist, and they are designated “R1” and “R2”, and “E1” and “E2”, respectively. “R1” and “E1” refer to the low deflection angles of Table 3, respectively. No “R0” or “E0” settings (zero values) exist because all spins were performed with the rudder and elevator deflected. The ailerons, however, do have an “A0” setting possible, which corresponds to no deflection. The “A1” and “A2” aileron settings, like those for the rudder and elevator, refer to the low and high deflection angles, respectively (see Table 3).

The second section of the naming convention consists of either an “Lft” or a “Rght.” This section is used to denote the direction in which the aircraft is spun when viewed from above. For an upright spin, an “Lft” indicates a rudder deflection to the left, and a corresponding upward deflection of the elevator. In the case of an inverted spin, an “Lft” indicates a rudder deflection in the pilot reference frame to the right, and a downward deflection of the rudder. When viewed from above in the viewer frame of reference, both an upright and inverted “Lft” spin will exhibit a rudder deflection to the left (nose left) and an upward elevator deflection (nose up). The third section of the naming convention defines whether the spin is an upright spin, or an inverted spin, denoted as “Up” and “Inv,” respectively.

The fourth and final section of the naming convention is not present for all spins. It is surrounded by parentheses, and serves as an additional note regarding the spin. If the ailerons were deflected in an anti-spin manner (i.e., right roll commanded in a left spin), a “cross ail” entry would be present within the parentheses. This term indicates that the airplane is in a cross-controlled situation. If no indication is present, and an “A0” is not present in the the first section of the name, then the ailerons are deflected in a pro-spin manner, an example of which would be a left roll commanded in a left spin. The other factor indicated by the fourth section would be the presence of a ventral fin. The terms “Fin 1”, “Fin 2”, and “Fin 3” are used to denote that ventral fins 1, 2, or 3, respectively, were present for that spin.

As an example, T2R1E1A1-Lft-Up-(cross ail) indicates that the spin configuration had a throttle setting of 750–1200 RPM, the rudder, elevator, and ailerons deflected at low deflection angles, in a left, upright spin, with the ailerons deflected in an anti-spin manner. The naming convention as described above is summarized in Table 5, and FS One™ RC flight simulator<sup>34</sup> renderings of the airplane with various control surface combinations are presented in Fig. 5.

When conducting flight tests, the winds aloft would produce a drift in the spin trajectory that would differ from day to day. In order to generate proper spin trajectories, the winds aloft were calculated and subtracted to produce a near-vertical spin trajectory. Figure 6(a) depicts the raw IMU trajectory information from a T0R1E1A0-Lft-Up spin, while Fig. 6(b) depicts that same spin trajectory with a calculated windfield removed. An average wind vector was determined for each spin and was subtracted from the raw data. This is why the plotted trajectories with the windfield subtracted are not perfectly straight, but are significantly straighter than that of the raw IMU data. In order to minimize the influence of the winds aloft and to have calm and steady winds in lieu of strong and gusty winds, flights were conducted near sunset on low-wind days.

The combination of the GPS resolution as recorded by the IMU, the small spin radii of the airplane, and the



Figure 5. Renderings of the spins using graphics from FS One: a) T0R1E1A0-Lft-Up, b) T0R1E1A0-Rght-Up, c) T0R1E1A1-Lft-Up, d) T0R1E1A1-Lft-Up(cross ail), e) T0R2E2A0-Lft-Up, f) T0R2E2A2-Lft-Up, g) T0R2E2A0-Rght-Up, h) T0R2E2A2-Rght-Up, i) T0R1E1A0-Lft-Inv, j) T0R1E1A1-Rght-Up, k) T0R1E1A1-Rght-Inv.

**Table 4. Throttle Settings and Approximate RPM Range in Spin**

Throttle Setting	Approximate RPM Range in Spin
T0	50–200
T1	340–840
T2	750–1200
Maximum	6900

**Table 5. Spin Configuration Naming Convention**

TREA Input	Spin Direction	Aircraft Orientation	Additional Note
T $\begin{pmatrix} 0 \\ 1 \\ 2 \end{pmatrix}$ R $\begin{pmatrix} 1 \\ 2 \end{pmatrix}$ E $\begin{pmatrix} 1 \\ 2 \end{pmatrix}$ A $\begin{pmatrix} 0 \\ 1 \\ 2 \end{pmatrix}$	$\begin{pmatrix} \text{Lft} \\ \text{Rght} \end{pmatrix}$	$\begin{pmatrix} \text{Up} \\ \text{Inv} \end{pmatrix}$	$\begin{pmatrix} \text{cross ail} \\ \text{Fin 1} \\ \text{Fin 2} \\ \text{Fin 3} \end{pmatrix}$

winds aloft prevented the spin radius from being accurately measured from the raw IMU position information. When stationary, the IMU was observed to demonstrate a resolution of 0.5 m in the  $x$ - and  $y$ -coordinates, which is too large of an error since the radii of the various spins were calculated to be on the order of 2 m. Instead of using the as-recorded  $x$ - $y$ - $z$  location of the IMU, for each spin, the  $x$ -,  $y$ -, and  $z$ -velocities were integrated using a 4-step backwards difference Adams-Bashforth method<sup>35</sup> as summarized by

$$k = 1 : y_{n+1} = y_n + hf_n \quad (5)$$

$$k = 2 : y_{n+1} = y_n + \frac{h}{2}(3f_n - f_{n-1}) \quad (6)$$

$$k = 3 : y_{n+1} = y_n + \frac{h}{12}(23f_n - 16f_{n-1} + 5f_{n-2}) \quad (7)$$

$$k = 4 : y_{n+1} = y_n + \frac{h}{24}(55f_n - 59f_{n-1} + 37f_{n-2} - 9f_{n-3}) \quad (8)$$

where  $h$  is the timestep,  $f_n$  values are the  $x$ -,  $y$ -, and  $z$ -velocities, and  $y_n$  values are the  $x$ -,  $y$ -, and  $z$ -coordinates. This integration method smoothed the data and allowed a 3D helix to become readily visible as shown in Fig. 7. All spin trajectories presented henceforth will have had the wind subtracted and the Adams-Bashforth integration applied.

The average bank angle, average pitch and its standard deviation, roll and yaw rates, vertical velocity, Reynolds number, spin parameter  $\omega$ , and spin radius were calculated for each of the spins, and those data are summarized in Table 6. The Reynolds number for each spin was determined using the pitot probe, as the velocity calculated from the IMU would include the effects of the windfield and not represent the true airspeed. All aerodynamic values were calculated for the temperature and pressure specific to the day and time of the flight test based on archived METAR data from nearby airports (KDEC and KCMI). Table 6 begins with the T0R1E1A0-Lft-Up spin, which was defined as the baseline spin and was used to demonstrate the repeatability of flight test results. The T0R1E1A0-Lft-Up spin represents the most-common configuration for which an airplane would typically enter an inadvertent stall/spin situation. The T0R1E1A0-Lft-Up spin would be encountered on a downwind-to-base or base-to-final traffic pattern turn that was overshoot where the pilot initiates an attempt to correct the overshoot by attempting to tighten the turn. The left rudder deflection was selected because a standard airport traffic pattern calls for left hand turns.<sup>36</sup> It should be noted that all spins performed in this series of flight tests were forced spins. After demonstrating the repeatability of flight test results, the effects of changing the direction (rudder deflection) of the spin, adding pro- or anti-spin aileron deflections, increasing the control surface deflections, inverting the spin, and increasing the motor power setting are investigated. The section concludes with an investigation of the effects of installing three different ventral fins for spin mitigation.

Because there is a limit to the flow incidence angle for which the pitot probe can accurately record dynamic pressure (20 deg), Figs. 9–30 all display the Reynolds number and angle of attack as calculated from the IMU total

velocity, even though this value will include the effects of the windfield. The plots are listed as “IMU  $\alpha$  (deg)” and “IMU Re,” respectively. The consistency of the IMU Reynolds number values between the three T0R1E1A0-Lft-Up spins of Figs. 9–10 shows that the flight test technique of planning flights near sunset on low-wind days, as mentioned before, was successful in achieving reasonably calm windfields on any given flight test day.

### A. Baseline Spin and Repeatability

Figures 9 and 10 compare three T0R1E1A0-Lft-Up spins flown on three different days; two different T0R1E1A0-Lft-Up spins (dashed blue line) are compared with the baseline spin (solid black line). It should be noted that the nearly-constant angle of attack as calculated from the pitot probe data suggests that this spin yielded too low of a velocity component parallel to the pitot probe for an accurate measurement to be made. As previously mentioned, the pitot probe is able to record dynamic pressures at flow angles of up to 20 deg. The Reynolds number as determined by the pitot-static system and the resulting angle of attack are approximately the same in Fig. 9 as shown in the upper right corner of the figures. No pitot probe data is presented for Case 3 of Fig. 10 because that spin was flown early in the flight test program when the testbed aircraft did not have a pitot probe installed. The plots of bank, pitch, and the roll, pitch, and yaw rates are approximately equal for all three T0R1E1A0-Lft-Up spins and demonstrate the repeatability of flight test results with the testbed aircraft. This repeatability is reinforced by the data of Table 6 where the vertical velocity of the spins was between 14.8 and 15.9 m/s.

### B. Direction of Spin

As demonstrated in Fig. 11, no significant differences between a T0R1E1A0-Lft-Up and T0R1E1A0-Rght-Up spin were observed. This suggests that while the propeller is windmilling during the spin, the effects of its spiral wake and small gyroscopic moments have no appreciable effect on the spin. The spin parameter for the T0R1E1A0-Rght-Up spin was 0.16 which agrees in regard to magnitude with the  $-0.20$  and  $-0.22$  of two of the T0R1E1A0-Lft-Up spins. The difference in sign is due to the different rudder deflection directions. Likewise, the bank and yaw rates were approximately equal and opposite, with a magnitudes of approximately 238 and 154 deg/s, respectively. The vertical velocity was slightly greater in magnitude at 16.8 m/s for the T0R1E1A0-Rght-Up spin when compared with the T0R1E1A0-Lft-Up spin average value of 15.5 m/s.

### C. Pro-Spin Aileron Deflection

Deflecting the ailerons in a pro-spin manner was observed to increase the magnitude of the bank angle from approximately zero (wings level) to  $-60.6$  deg while not significantly affecting the pitch angle. As seen in Fig. 12, the addition of pro-spin ailerons increased the Reynolds number as well as the magnitude of the roll rate. The T0R1E1A0-Lft-Up pitch rate of 0 deg/s was increased to over 150 deg/s for the T0R1E1A1-Lft-Up spin while the yaw rate was decreased in magnitude from approximately  $-155$  to  $-101.0$  deg/s. A corresponding decrease in the magnitude of the spin parameter resulted from this lower yaw rate, reducing the value from  $-0.22$  to  $-0.08$  as seen in Table 6. Due to this lower yaw rate, the time required for a recovery from the spin yaw rate to a zero yaw rate decreased through the addition of pro-spin ailerons. A downside to the addition of pro-spin ailerons is, however, an increased descent rate as seen in Table 6, where the descent rate increases from 16.8 m/s for the T0R1E1A0-Rght-Up spin to 24.7 m/s for the T0R1E1A1-Rght-Up spin; a similar increase from approximately 16 m/s to 25.4 m/s was noted for the T0R1E1A0-Lft-Up and T0R1E1A1-Lft-Up spins, respectively. The increased descent rate of the pro-spin aileron spins when compared with the neutral aileron spins coupled with the decreased yaw rate reduces the magnitude of the spin parameter for both left and right spins from around 0.20 to 0.08.

Table 6. Summary of Individual Spin Parameters

Spin	$\phi_{avg}$ (deg)	$\theta_{avg}$ (deg)	$\sigma_{\theta}$	$p_{avg}$ (deg/s)	$r_{avg}$ (deg/s)	$V_z$ (m/s)	$Re$	$\omega$	$R_s$ (m)	Fig.
TORIE1A0-Lft-Up	0.7	-56.6	3.6	-238.1	-158.9	-15.9	$0.65 \times 10^6$	-0.20	1.93	9, 10
TORIE1A0-Lft-Up	1.0	-55.8	4.8	-232.7	-157.4	-14.8	$0.58 \times 10^6$	-0.22	1.91	9
TORIE1A0-Lft-Up	0.2	-57.4	3.3	-235.3	-150.3	-15.7	$n/a$	-0.20	2.23	10
TORIE1A0-Rght-Up	-1.3	-56.7	5.3	239.6	157.9	-16.8	$0.65 \times 10^6$	0.16	1.97	11
TORIE1A1-Lft-Up	-60.6	-59.1	10.9	-355.1	-101.0	-25.4	$1.03 \times 10^6$	-0.08	5.27	12
TORIE1A1-Lft-Up-(cross ail)	13.1	-46.4	2.0	-186.9	-174.5	-14.0	$0.50 \times 10^6$	-0.28	1.11	13
TOR2E2A0-Lft-Up	-11.2	-48.1	5.6	-134.7	-119.2	-14.2	$1.01 \times 10^6$	-0.10	2.52	14
TOR2E2A2-Lft-Up*	-53.5	-40.8	14.5	-182.8	-77.9	-14.0	$0.55 \times 10^6$	-0.64	4.57	15, 17
TOR2E2A0-Rght-Up	16.7	-53.8	4.6	182.2	129.3	-16.4	$0.64 \times 10^6$	0.16	2.63	16
TOR2E2A2-Rght-Up*	47.1	-38.7	17.4	178.4	86.3	-15.7	$0.55 \times 10^6$	0.71	3.47	16, 17
TORIE1A0-Lft-Inv	-12.3	-63.2	12.8	266.3	-106.1	-21.1	$0.83 \times 10^6$	-0.10	5.66	18
TORIE1A1-Rght-Up	56.6	-59.3	13.5	383.9	107.8	-24.7	$1.01 \times 10^6$	0.08	4.67	19
TORIE1A1-Rght-Inv	-2.9	-56.6	12.5	259.5	154.6	-20.9	$0.84 \times 10^6$	0.11	2.04	19
TIRIE1A0-Lft-Up	-4.6	-57.3	3.8	-234.8	-151.6	-16.9	$0.64 \times 10^6$	-0.19	2.18	20
T2RIE1A0-Lft-Up	-12.3	-59.7	3.9	-264.2	-152.6	-19.6	$0.77 \times 10^6$	-0.16	2.37	21
T2RIE1A0-Rght-Up	-4.4	-57.1	6.6	248.7	161.3	-17.7	$0.68 \times 10^6$	0.19	1.91	22
TIRIE1A1-Lft-Up	-59.1	-61.3	4.5	-365.3	-104.5	-23.5	$0.85 \times 10^6$	-0.10	5.38	23
TIRIE1A1-Rght-Up	57.4	-63.0	7.5	396.5	111.0	-25.2	$0.90 \times 10^6$	0.10	5.12	24
TIRIE1A1-Lft-Up-(cross ail)	5.2	-39.8	3.6	-147.0	-178.3	-16.0	$0.56 \times 10^6$	-0.25	0.84	25
TORIE1A1-Lft-Up-(Fin 1)	-58.5	-60.6	3.6	-352.8	-104.0	-24.2	$0.96 \times 10^6$	-0.10	5.29	26
TORIE1A1-Lft-Up-(Fin 2)	-58.5	-58.3	11.8	-357.0	-104.8	-25.0	$0.98 \times 10^6$	-0.06	4.78	27
TORIE1A1-Lft-Up-(Fin 3)	-52.2	-53.2	17.3	-352.8	-102.7	-28.5	$1.08 \times 10^6$	-0.07	4.07	28
TIRIE1A1-Lft-Up-(Fin 3)	-47.4	-48.3	20.1	-352.5	-103.1	-30.1	$1.12 \times 10^6$	-0.07	3.40	29
TORIE1A0-Lft-Up-(Fin 3)	-1.3	-57.4	9.0	-233.1	-145.8	-17.6	$0.62 \times 10^6$	-0.13	2.36	30

\*gyrating spin

#### **D. Anti-Spin Aileron Deflection**

Figure 13 demonstrates the effects of adding anti-spin aileron deflection to a T0R1E1A0-Lft-Up spin configuration. The addition of anti-spin aileron is the typical reaction of an untrained pilot to the entry of a stall/spin situation and will further aggravate the spin by placing the airplane in a cross-controlled situation, hence the “cross ail” moniker to denote this spin configuration. In a left spin, by more deeply stalling the left wing, the airplane appears to enter a more stable and thus less recoverable spin mode. The more stable spin mode is evidenced by the smaller magnitude of the oscillations in the bank and pitch as well as the slower recoveries to the bank, pitch, and roll rates. The decrease in the recovery rates due to the addition of anti-spin ailerons is a significant result and illustrates why proper spin training is essential; the reaction of an untrained pilot to a stall/spin situation would be to rotate the control column opposite of the spin, i.e., command anti-spin ailerons. Onboard video from the testbed aircraft and the first author’s own full-scale spin training demonstrate that the view from the cockpit during a spin consists of a near 90-deg nose down attitude with an apparent high-rate roll in the direction of the spin. The addition of anti-spin ailerons yielded a slight increase in the magnitude of the yaw rate to  $-174.5$  deg/s. The spin parameter was consequently increased in magnitude from  $-0.20$  to  $-0.28$ , while the vertical velocity was decreased in magnitude to  $-14.0$  m/s by the anti-spin aileron deflection.

Despite numerous attempts on different days with different pressures and temperatures, the airplane would always exit a right spin when anti-spin (left roll) ailerons were applied. It should also be noted that with the installation of any of the ventral fins, the addition of anti-spin ailerons to the left spin would cause the airplane to exit the spin. In short, this aggravated spin was only able to be performed in a left spin with no ventral fin installed.

#### **E. Increased Control Surface Deflections (with and without ailerons)**

Increasing the control surface deflections from the low rate to the high rates (see Table 3) reduced the magnitude of the roll and yaw rates with neutral ailerons from  $-235$  deg/s and  $150$  deg/s to  $-134.7$  deg/s and  $-119.2$  deg/s, respectively; a minor effect on the pitch rate was also noted in Fig. 14. The average pitch angle was reduced in magnitude from  $-57$  to  $-48$  deg, but no significant changes to the recovery were observed or experienced.

The addition of ailerons to a high deflection rate spin (T0R2E2A0-Lft-Up to T0R2E2A2-Lft-Up spin) significantly altered the motion of the spin. As shown in Fig. 15, a periodic unsteady gyration was introduced to the spin motion through the addition of ailerons to a high deflection rate spin. The periodic motion exhibited a period of approximately 2.5 s and was repeatable in different wind conditions. The period remained nearly unchanged for spins to the right as shown in Fig. 16. When the right and left high deflection pro-spin aileron spins are compared, as shown in Fig. 17, it becomes evident that the spin to the left has a slightly longer period than the right hand spin. Even though this difference is minor, it is most likely due to a slight asymmetry in the airframe construction. Airframe asymmetry is hypothesized to be the case because the atmospheric conditions were nearly identical between the two flights. The temperature on both days of these spins was 29 deg C and the pressure differed by only 0.01 mmHg. Both the left and right spins exhibit the same double peak for the yaw rate and pitch, with the yaw rate being approximately equal and opposite for the left and right spins. No pitot-static data is presented in Fig. 17 because these spins were flown prior to the installation of the pitot probe on the Aero Testbed.

Both the right and left high deflection spins with pro-spin ailerons demonstrated the same highly regular periodic gyration motion. This motion was characterized by a period of approximately 2.5 s, a buildup in pitch rate followed by a steep dropoff from the maximum, and a double peak in the yaw rate in each period. Figure 8(a) depicts a T0R2E2A2-Lft-Up spin trajectory with the aircraft magnified four times and drawn every 0.5 s.

#### **F. Inverted Spin (with and without ailerons)**

Inverting the spin for an aileron neutral spin reduces the yaw rate and destabilizes the spin as evidenced by the larger oscillations in bank and pitch in Fig. 18. The pitch angle is slightly increased in the negative direction and more rapid recoveries are apparent for the bank and heading rates as well as the pitch angle. Additionally, as shown in the beginning phase of the spin, the bank and yaw rates approach their maximum near steady-state values at a slower rate than when compared with the level flight case. It should also be noted that the direction of the bank changes; this direction change is an artifact of the inverted orientation of the spin entry. The rudder is deflected in the same direction for both spins, but in the level spin, the left wing stalls and drops, creating a roll to the left. In the inverted spin case when observed from the airplane frame of reference, the left wing stalls while inverted, creating a roll to the right. This spin was studied because it was a close approximation to inverting the tail geometry and changing the shape of the aft fuselage from a flat-bottom round-top geometry to a round-bottom flat-top geometry. The round-bottom fuselage

geometry is preferable as described in the literature.<sup>15,20,21</sup> These inverted spins were studied because the testbed airplane has zero dihedral, zero incidence angle between the wing and horizontal stabilizer, and symmetric airfoils for both the wing and the horizontal stabilizer, so no effects from dihedral or different airfoils would be encountered. It should be noted that when upright, the horizontal stabilizer is located 3.1 cm (1.2 in) above the wing; when inverted, the horizontal stabilizer is located 3.1 cm (1.2 in) beneath the wing.

While Fig. 18 addresses the inverting of an aileron neutral spin, Fig. 19 shows the effects of inverting a spin with pro-spin ailerons. In this case, inverting the aileron-on spin reduces the measured pitch rate to zero and reduces the bank rate slightly while increasing the yaw rate. The average bank is slightly reduced while no appreciable change to the pitch is observed. The combination of reduced bank rate and increased yaw rate may be attributable to the new vertical tail “geometry” where the increased vertical tail area beneath the horizontal stabilizer acts as a sort of keel while the increased rudder area increases the moment and thus effectiveness of the rudder. Inverting the T1R1E1A0-Lft-Up spin also reduces the spin parameter by nearly 50% from  $-0.20$  for the T0R1E1A0-Lft-Up spin to  $-0.10$  for the T0R1E1A0-Lft-Inv spin. Figure 8(b) depicts a T1R1E1A0-Lft-Inv spin trajectory with the aircraft magnified four times and drawn every 0.5 s.

### G. Effect of Motor Power / Throttle

As visible in Fig. 20, increasing the throttle from an idle setting (T0) to one that will produce an RPM of 340–840 (T1) has no appreciable effect on a spin with neutral ailerons. This observation is verified by the data of Table 6, where the T0R1E1A0-Lft-Up and T1R1E1A0-Lft-Up spins have spin parameters of  $-0.20$  and  $-0.19$ , respectively. The pitch, roll rate, yaw rate, and Reynolds number values also do not change appreciably, but the descent rate was observed to increase to 16.9 m/s in Table 6. The descent rate for the T1R1E1A0-Lft-Up spin configuration was, however, nearly equal to the descent rate for the T0R1E1A0-Rght-Up spin. If one observation were to be made between the T0R1E1A0-Lft-Up and T1R1E1A0-Lft-Up spins, it would be the slight reduction in the rate of recovery of the yaw rate for the T1R1E1A0-Lft-Up spin. Increasing the motor power to a setting that would produce an RPM of 750–1200 (T2) as shown in Fig. 21 did increase the Reynolds number, pitch rate, and slowed the recovery from the steady-state spin yaw rate in a left hand spin. Noting that the slowed recovery from the spin yaw rate was less-pronounced in Fig. 20, it is hypothesized that this change is not due to the aerodynamic effects of the propeller, but due to the gyroscopic effects. A rotating propeller produces an increasingly-left turning tendency as the motor power setting is raised. This is in-theory confirmed in Fig. 22 where no significant changes to the spin are observed aside from a slight increase in the recovery from the spin yaw rate.

Additional changes introduced when progressing from the T0R1E1A0-Lft-Up to T1R1E1A0-Lft-Up and T2R1E1A0-Lft-Up spins are an increase in the negative direction of the bank angle from approximately 0 to  $-4.6$  deg and  $-12.3$  deg, respectively. The pitch angle of the T2R1E1A0-Lft-Up spin is also increased in the negative direction to  $-59.7$  deg, and the roll rate is increased by approximately 12%. The descent rate of the T2R1E1A0-Lft-Up spin is increased from the T0R1E1A0-Lft-Up spin to 19.6 m/s, and consequently the spin parameter decreases in magnitude.

When power is added to a spin with pro-spin ailerons as depicted in Fig. 23, the only appreciable effect is the apparent stabilization of the spin as evidenced by decreased oscillations in the bank and pitch values. The case of the right spin, as shown in Fig. 24 also demonstrates this decreased magnitude of oscillation in the bank and pitch spin values. Once again, the propeller effects appear to have a small influence, as the left spin recovery is slightly slowed and the right spin recovery is slightly accelerated.

A significant motor RPM effect was observed for a left spin with aggravated ailerons as shown in Fig. 25. When the throttle setting was increased from “T0” to “T1” (see Table 4), the recovery time increased from approximately 2 to 4 s and required 2.5 turns of the aircraft before the yawing and rolling ceased. Recoveries from all spins were initiated by removing all control inputs and then initiating a gentle motor-idle (“T0”) pullout with wings level in order to keep the load factor experienced by the airplane as low as possible. The aggravated spin was reported to take 1–1.5 turns before a recovery could be initiated while the increase in throttle from “T0” to “T1” required an additional 2.5 turns before the initiation of the recovery could be performed.

### H. Effect of Ventral Fins 1, 2, and 3

Figure 26 compares T0R1E1A1-Lft-Up spins with and without Ventral Fin 1 installed. A drawing of the three fins and their installed location on the aircraft is presented in Fig. 2(b). No significant differences are apparent in Fig. 26, but Table 6 shows that the yaw rate was reduced from  $-129.3$  to  $-104.0$  deg/s, and the spin parameter decreased in magnitude to  $-0.10$ . Extending Fin 1 forward yielded Fin 2, and the results of the installation of Fin 2 are presented in Fig. 27. The spin parameter for the T0R1E1A1-Lft-Up-(Fin 1) and T0R1E1A1-Lft-Up-(Fin 2) spins are the same, and

comparing two spins in Table 6 does not show any significant differences aside from a slight increase in the descent rate and Reynolds number.

Fin 3 was the same length as Fin 1, but was 1-in taller, and a comparison of the T0R1E1A1-Lft-Up and T0R1E1A1-Lft-Up-Fin 3) spins is shown in Fig. 28. A more rapid recovery from the spin roll and yaw rates was visible in Fig 28. The Reynolds number in the spin was increased, and consequently the spin parameter was decreased in magnitude from  $-0.08$  to  $-0.07$ . The pitch angle was decreased in magnitude from  $-53.8$  to  $-48.3$  deg. The magnitude of both the pitch and bank oscillations were significantly increased with the addition of Fin 3, suggesting that the spin was less stable. Shedding further light on the Fin 3 installation is Fig. 29 which shows the differences created by installing Fin 3 for a left pro-spin aileron spin with a “T1” throttle setting. The addition of motor power significantly increases the magnitude of the bank and pitch oscillations and once again the recovery from the yaw rate is increased through the addition of Fin 3. A slight increase in the pitch rate and a slight decrease in the bank rate were also observed. A small increase in the descent rate to 30.1 m/s was observed in Table 6 with no significant change in the magnitude of the spin parameter.

The final investigation examined the effects of Fin 3 in an aileron neutral spin (T0R1E1A0-Lft-Up) as shown in Fig. 30. Once again, a clear increase in the rate of recovery of the yaw and bank rates is observed with Fin 3. The yaw rate and spin parameter of the developed spin were slightly decreased for the Fin 3 case, to  $-145.8$  deg/s and  $-1.10$ , respectively. Additionally, the change in pitch from the developed spin to one from which a recovery pullout could be initiated was much quicker when Fin 3 was installed.

A final observation that was noted for all installed ventral fins was that they removed the ability of the airplane to spin with anti-spin ailerons. On all test flights and for all ventral fins, the airplane would immediately exit the spin if anti-spin ailerons were commanded. The exiting of the spin through anti-spin ailerons is in contrast to the no-fin configuration of the airplane, which would (only) spin to the left with anti-spin ailerons and demonstrated the slowest recovery of any of the spins.

## V. Conclusions

An experimental flight test study was performed to investigate the effects of various control surface deflections and combinations, motor power settings, and orientations on the spin characteristics of a single-engine subscale aircraft. Additionally, the spin mitigation and recovery effectiveness of three different ventral fin configurations was tested. The repeatability of flight test results was demonstrated, and the flight vehicle and instrumentation experimental setup was validated to provide proper data. By testing spins on a large yet subscale testbed airplane, actual pilots and expensive full-size airframes are not put in danger. Additionally, some of the Reynolds number effects that are encountered when scaling up results from 10%-scale spin-tunnel models may be avoided.

The results indicate that a ventral fin is able to aid in the recovery from spin of a single-engine aircraft through the reduction of the roll rate, an increase in the Reynolds number, a decrease in the pitch, and a decrease in the spin parameter. It was also shown that these ventral fins allowed the specific subscale testbed aircraft the ability to exit a spin by means of deflecting anti-spin ailerons. The results also indicate that the increase in propeller RPM adversely affects the recovery from a left spin, especially when the ailerons are directed in an anti-spin manner.

## VI. Acknowledgments

The authors would like to thank Craig Pauga, Agrim Sareen, Gustavo Fujiwara, and Ayo Adesida for their help with supporting the test flights, and Agrim Sareen for his additional help with portions of the initial development of the MATLAB code used to load and plot the raw IMU data. The authors would also like to thank Horizon Hobby, specifically Michael McConville for providing design data and CAD drawings for his Extra 260 aircraft design and David Ribbe for initial aircraft checkout and for first test flights, and the Monticello Model Masters RC Club for allowing the use of Eli Field.

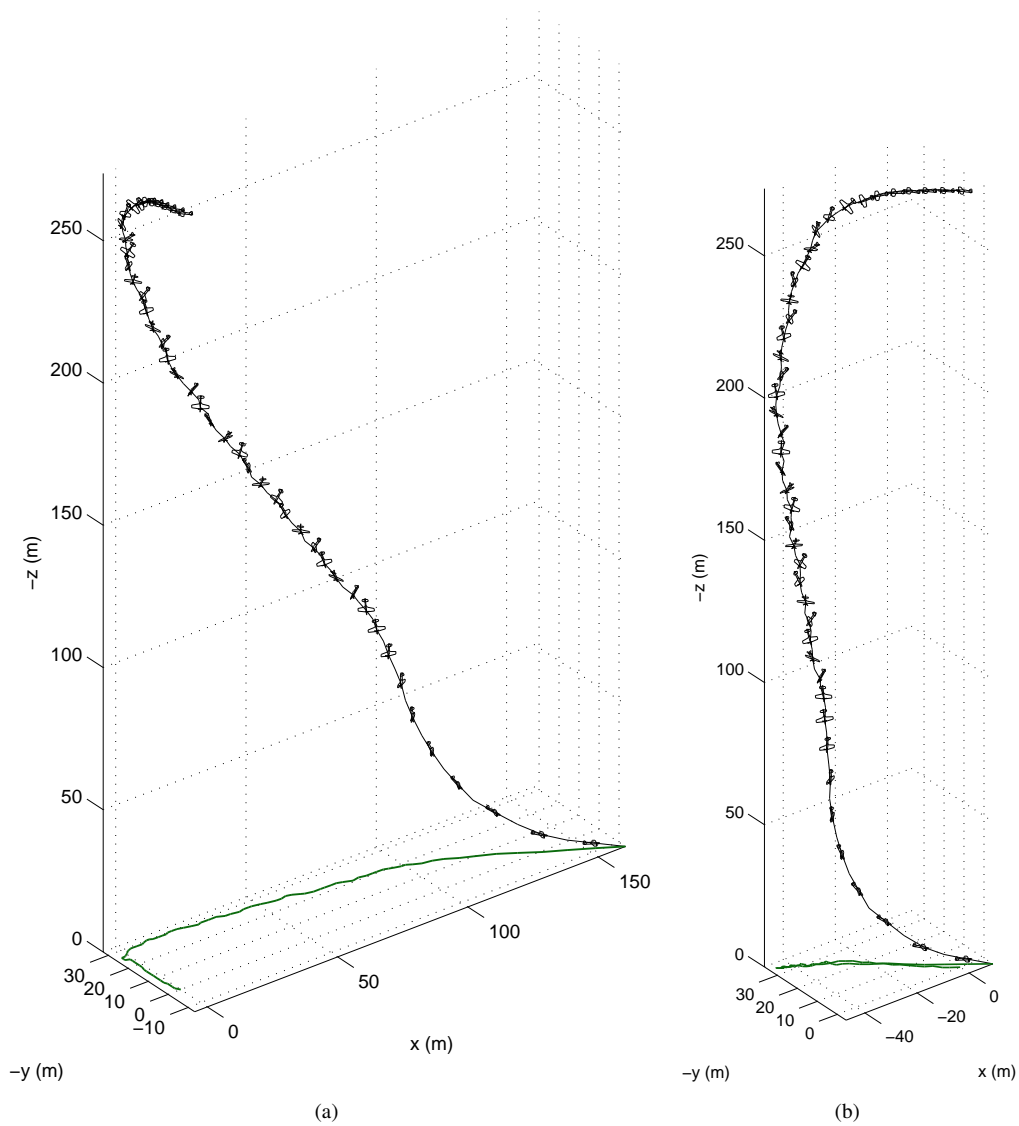


Figure 6. TOR1E1A0-Lft-Up spin trajectories for (a) raw IMU data, and (b) IMU trajectory with windfield subtracted [aircraft magnified three times actual size and drawn every 0.40 s].

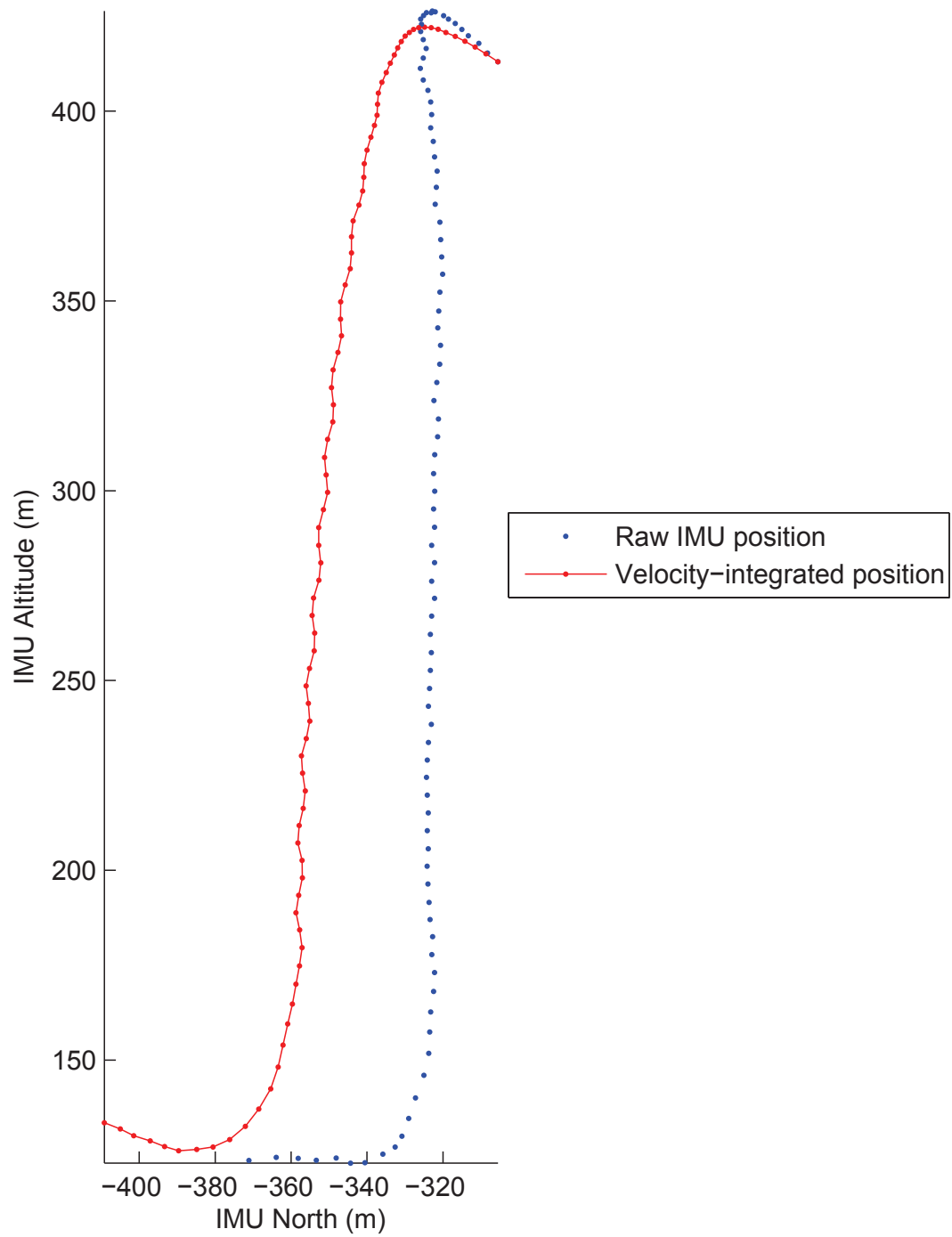


Figure 7. Plot of raw IMU position (blue) and position integrated from IMU velocities (red).

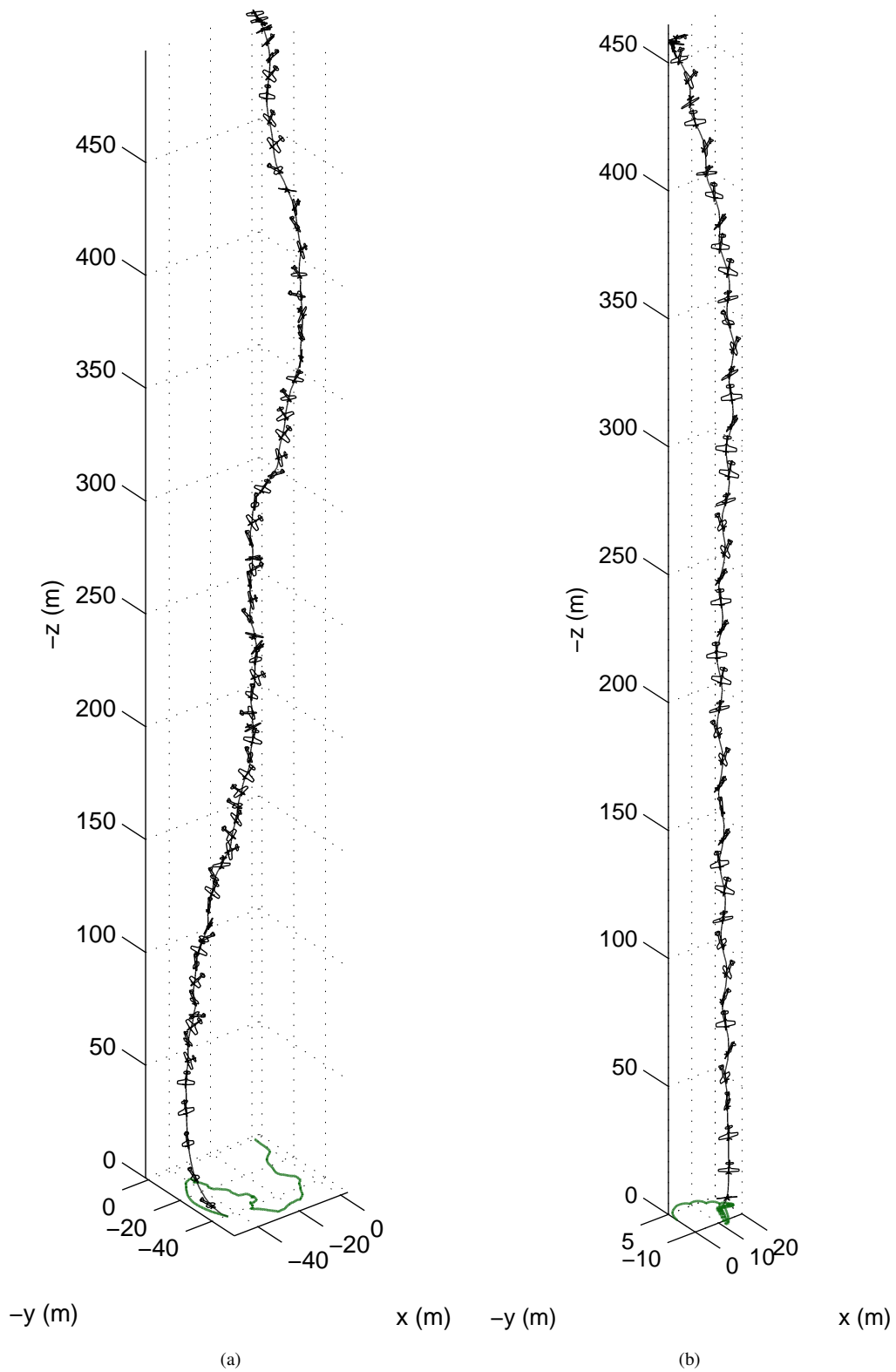


Figure 8. Spin trajectories for (a) T0R2E2A2-Lft-Up, and (b) T0R1E1A0-Left-Inv spins with windfield subtracted [aircraft magnified four times actual size and drawn every 0.50 s].

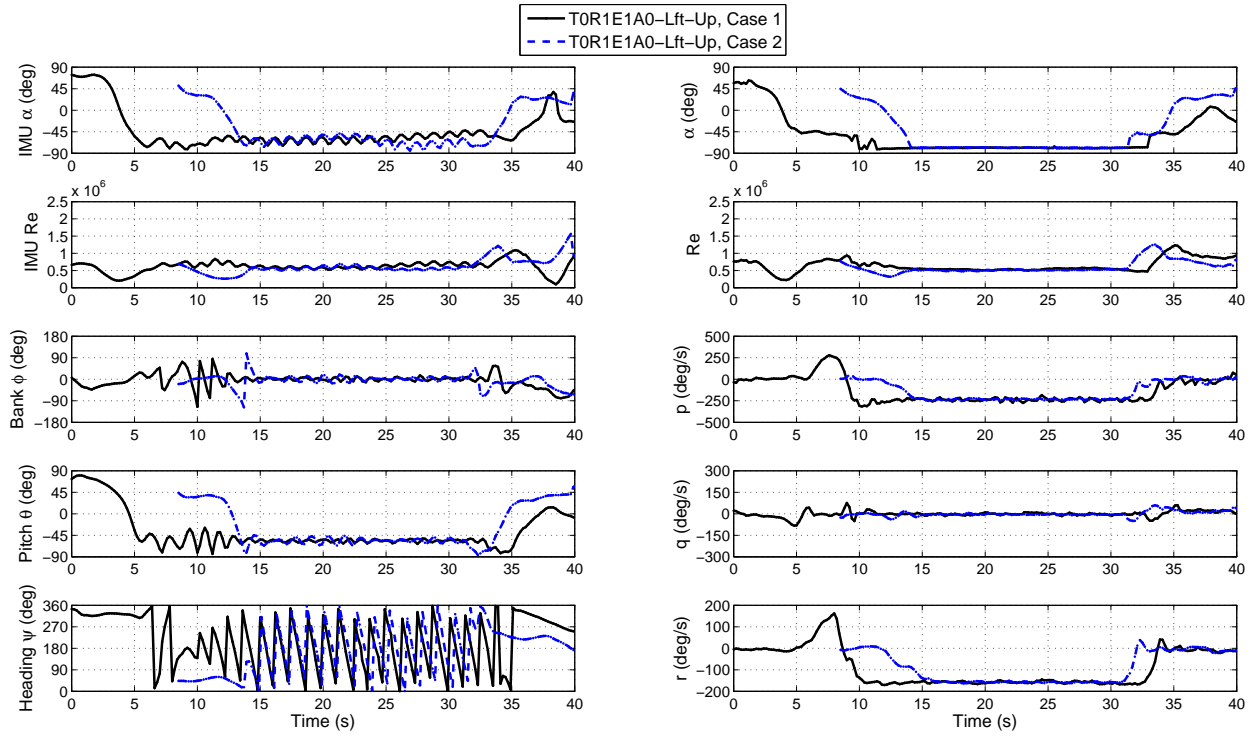


Figure 9. Two T0R1E1A0-Lft-Up spins performed on different days (repeatability test).

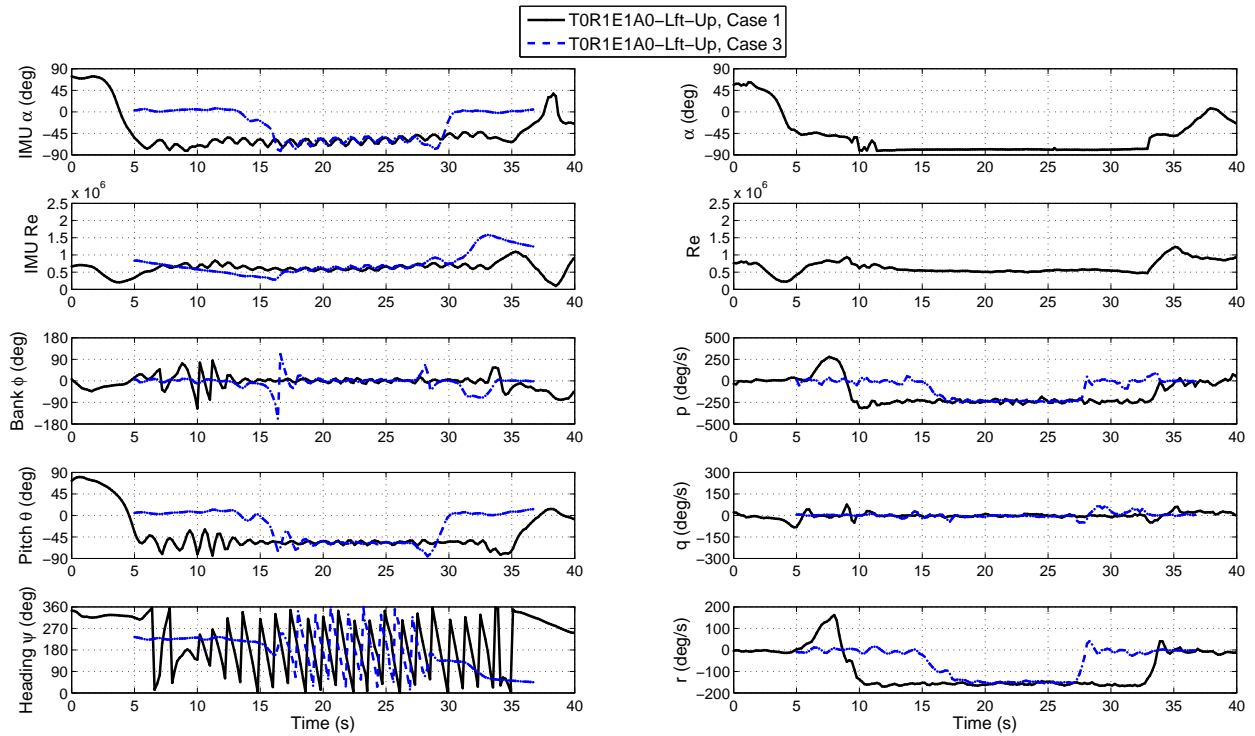


Figure 10. Two T0R1E1A0-Lft-Up spins performed on different days (repeatability test).

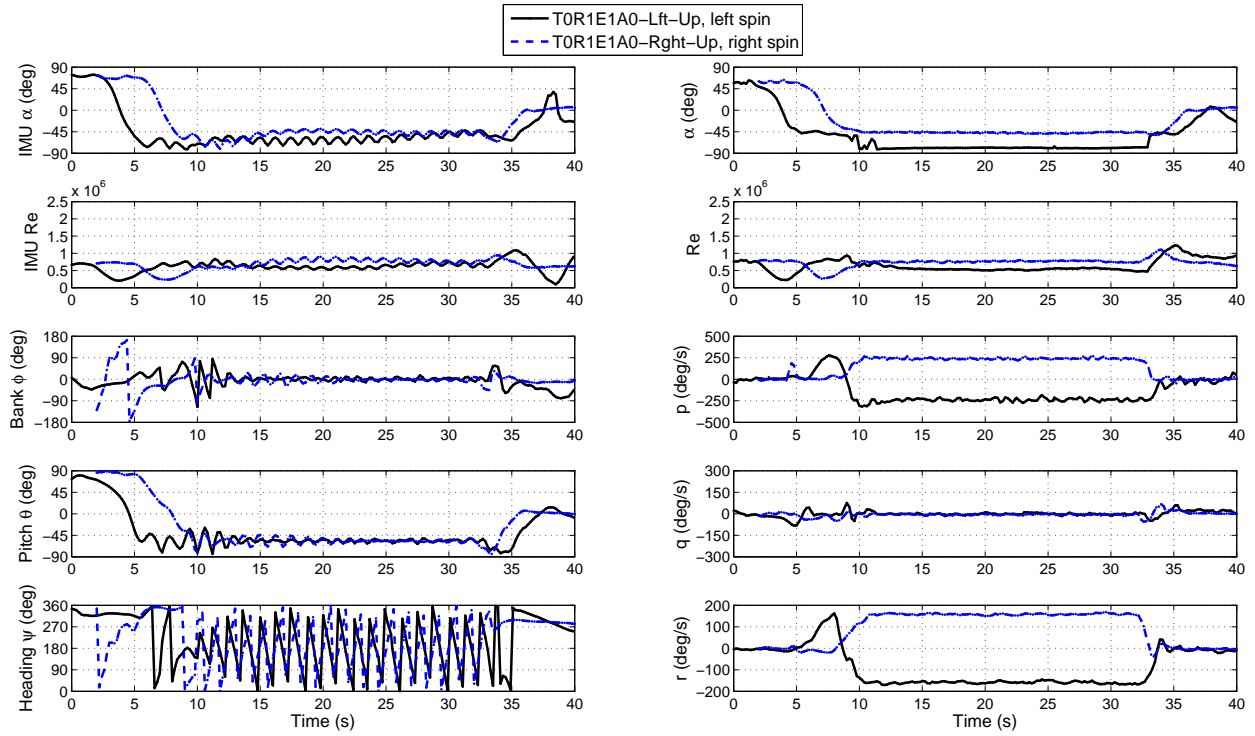


Figure 11. T0R1E1A0-Lft-Up and T0R1E1A0-Rght-Up spins performed on two different flights (effect of spin direction).

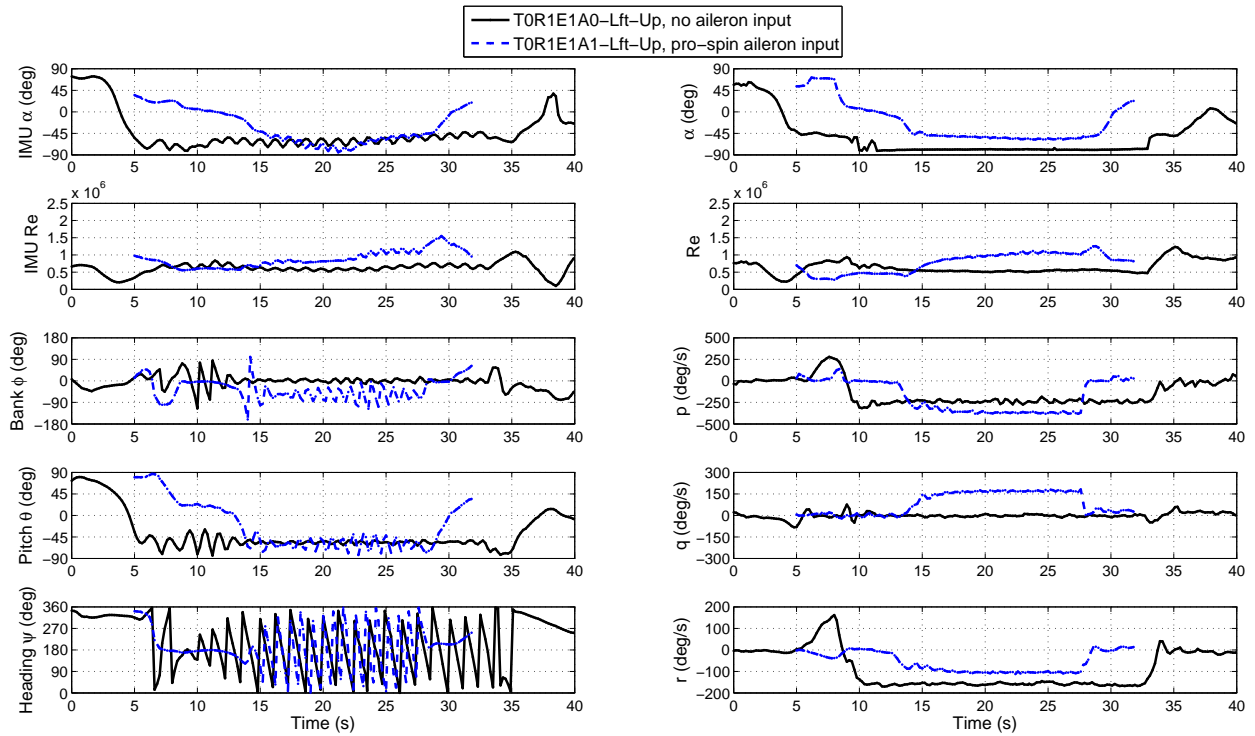


Figure 12. T0R1E1A0-Lft-Up and T0R1E1A1-Lft-Up spins performed on two different days (effect of pro-spin aileron input).

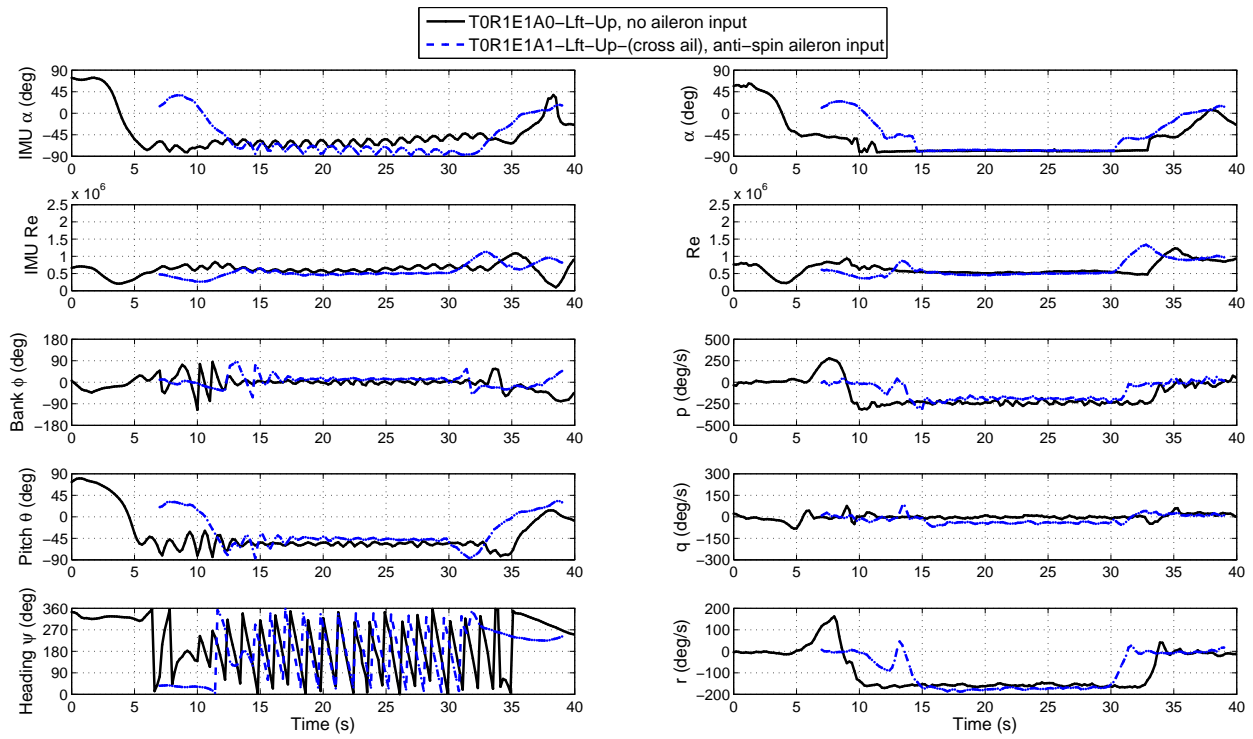


Figure 13. T0R1E1A0-Lft-Up and T0R1E1A1-Lft-Up-(cross ail) spins performed on two different days (effect of anti-spin aileron input).

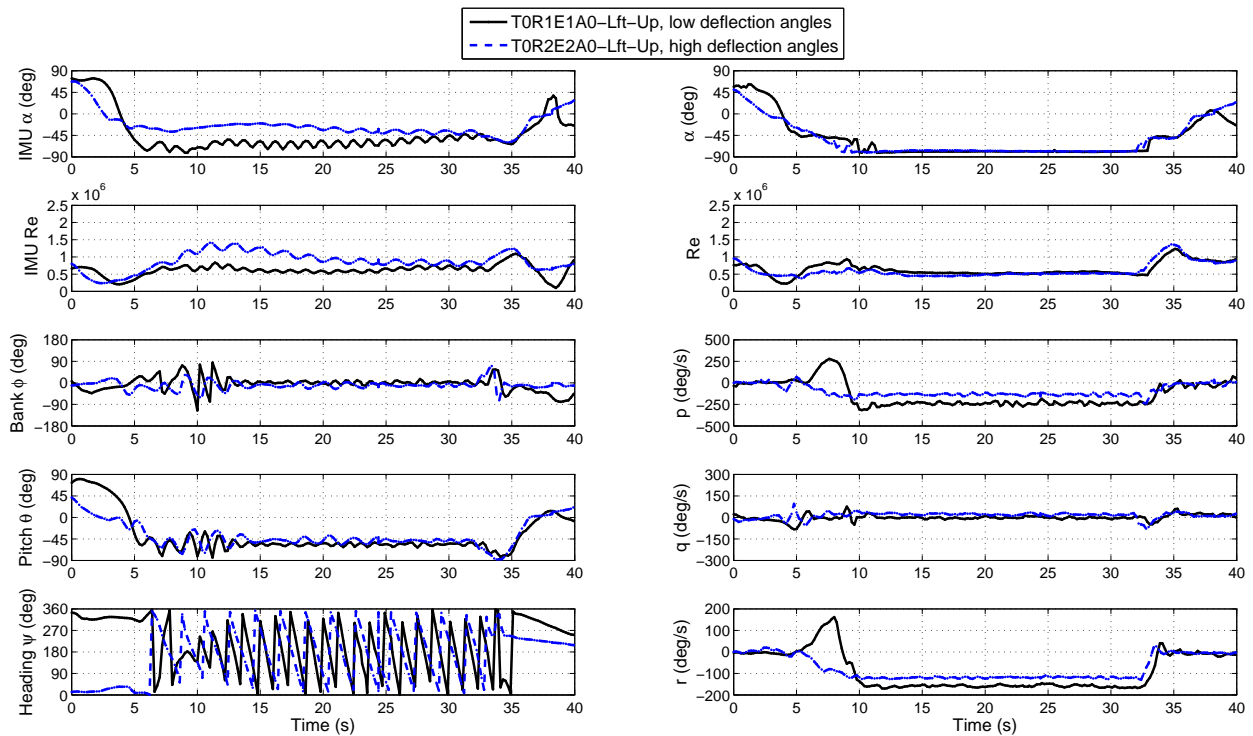


Figure 14. T0R1E1A0-Lft-Up and T0R2E2A0-Lft-Up spins performed on two different days (effect of high deflection angles).

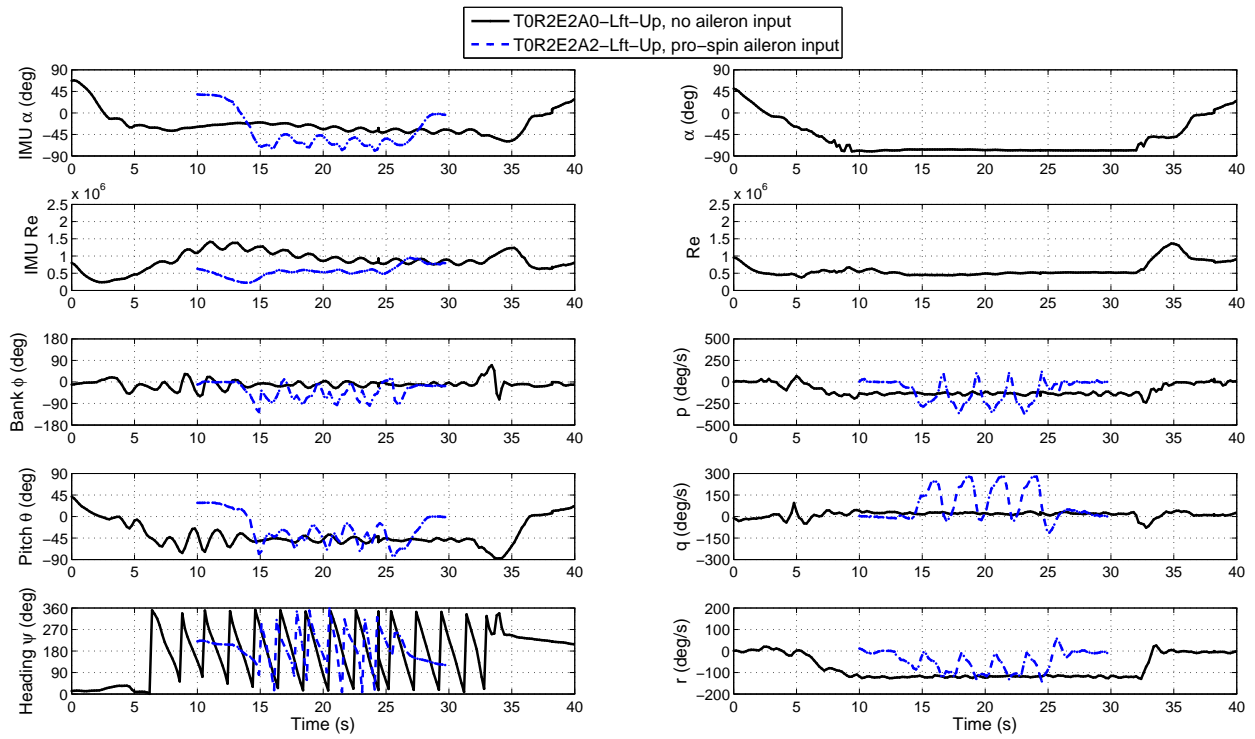


Figure 15. T0R2E2A0-Lft-Up and T0R2E2A2-Lft-Up spins performed on two different days (effect of pro-spin aileron input at high deflection angles).

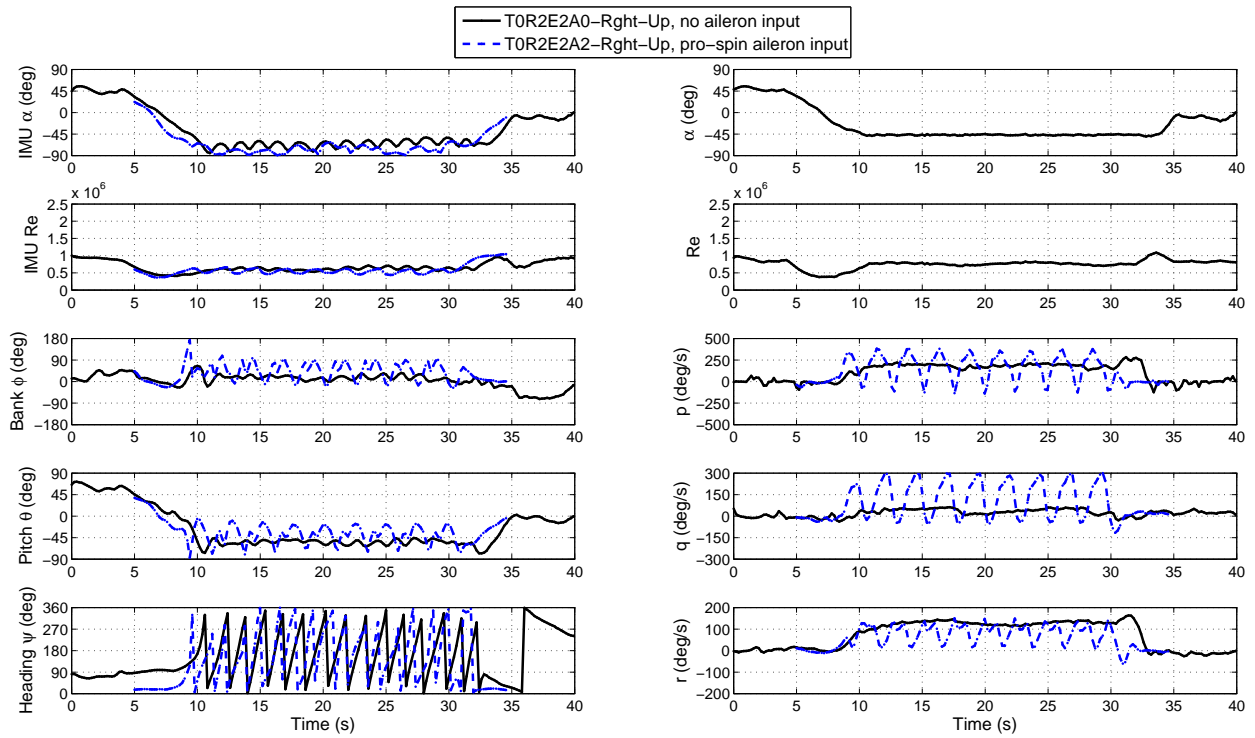


Figure 16. T0R2E2A0-Rght-Up and T0R2E2A2-Rght-Up spins performed on two different days (effect of pro-spin aileron input at high deflection angles).

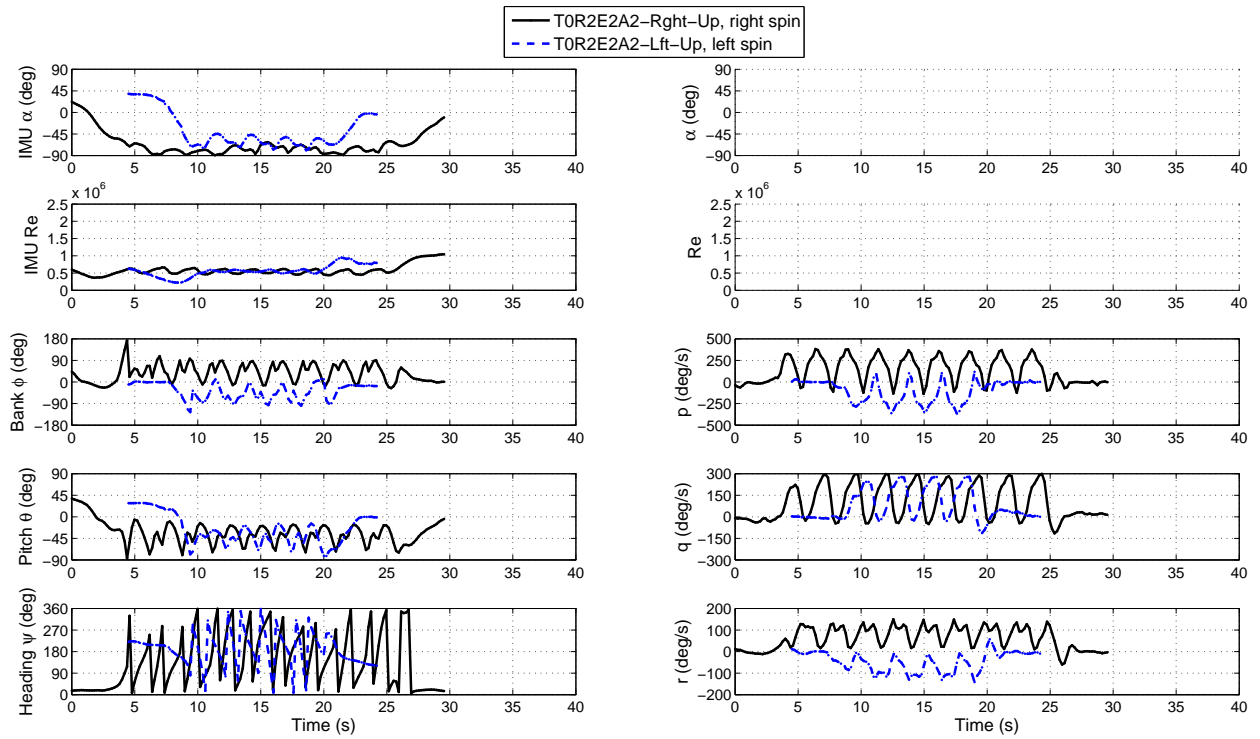


Figure 17. T0R2E2A2-Right-Up and T0R2E2A2-Lft-Up spins performed on two different days (effect of spin direction at high deflection angles).

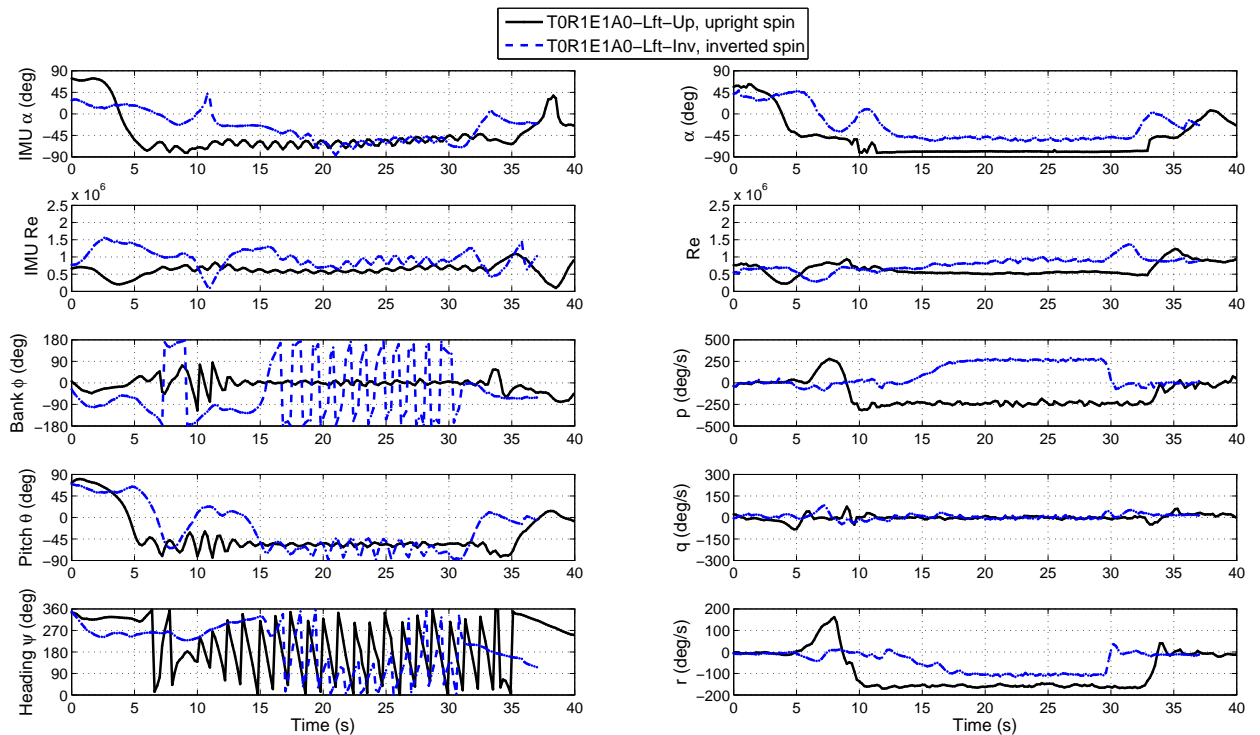


Figure 18. T0R1E1A0-Lft-Up and T0R1E1A0-Lft-Inv spins performed on two different days (effect of inverted spin).

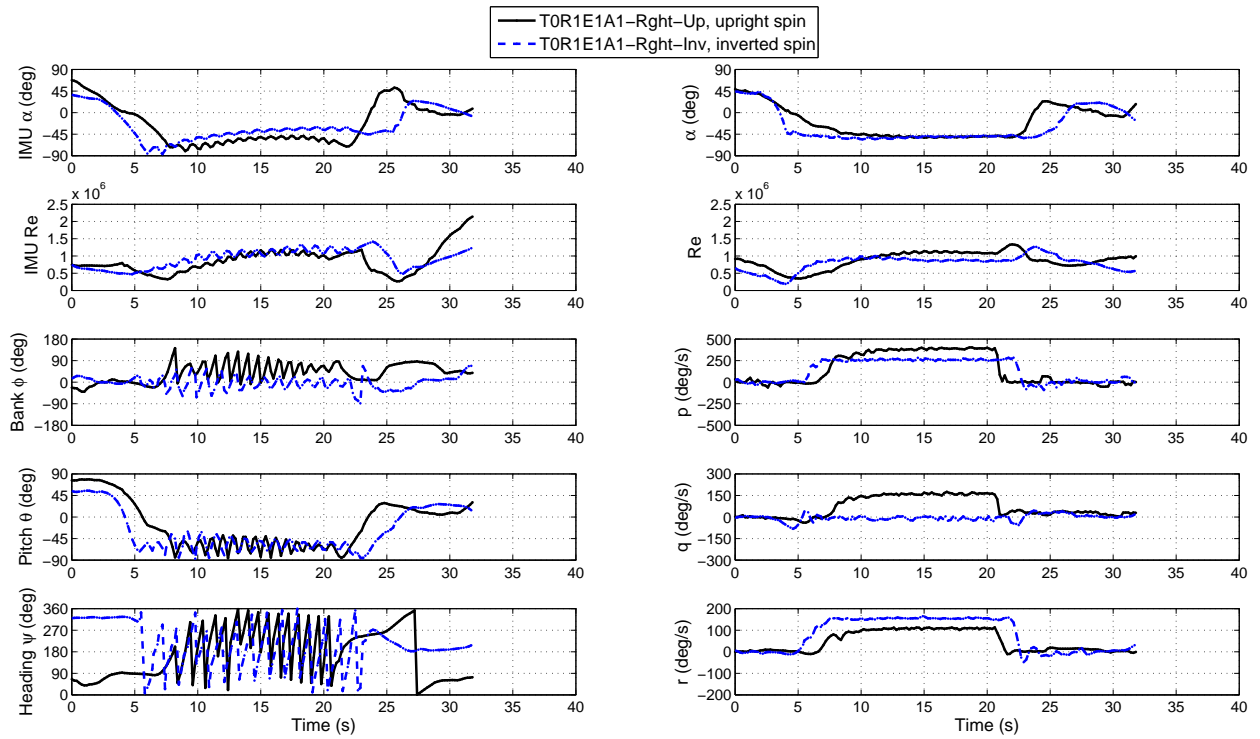


Figure 19. T0R1E1A1-Right-Up and T0R1E1A1-Right-Inv spins performed on two different flights (effect of inverted spin with pro-spin ailerons).

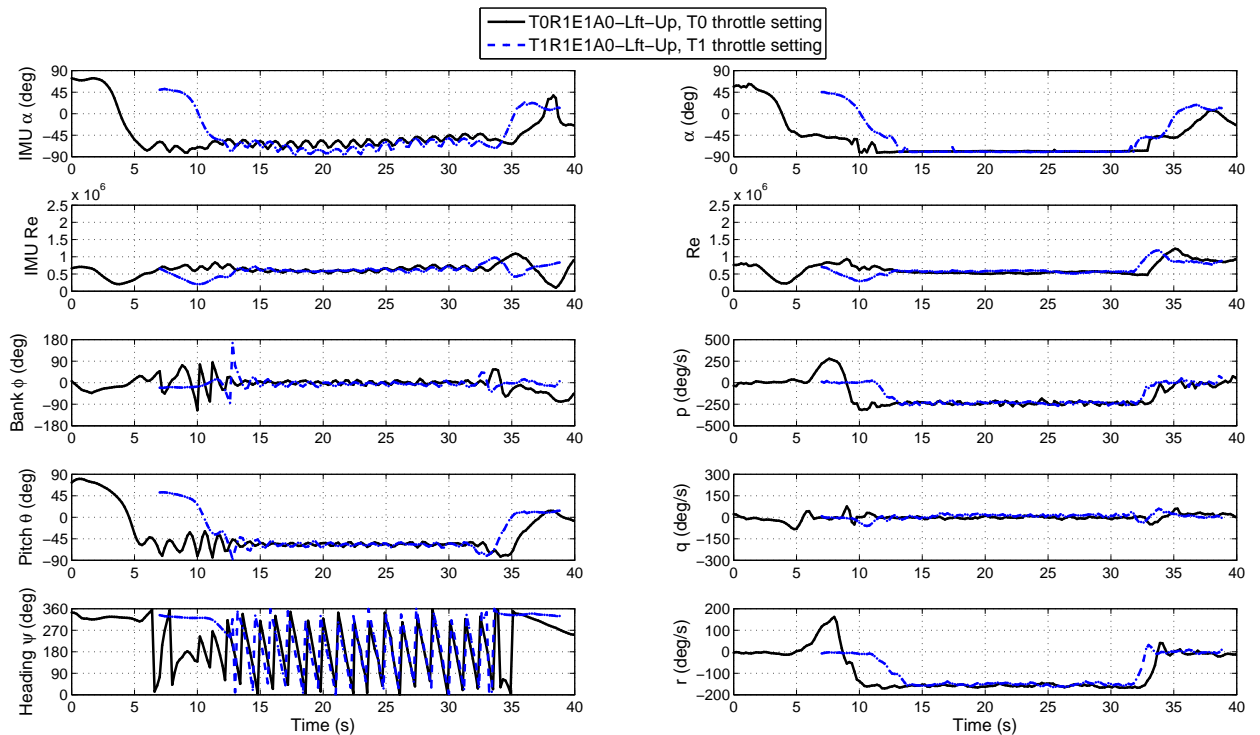


Figure 20. T0R1E1A0-Lft-Up and T1R1E1A0-Lft-Up spins performed on the same flight (effect of throttle setting).

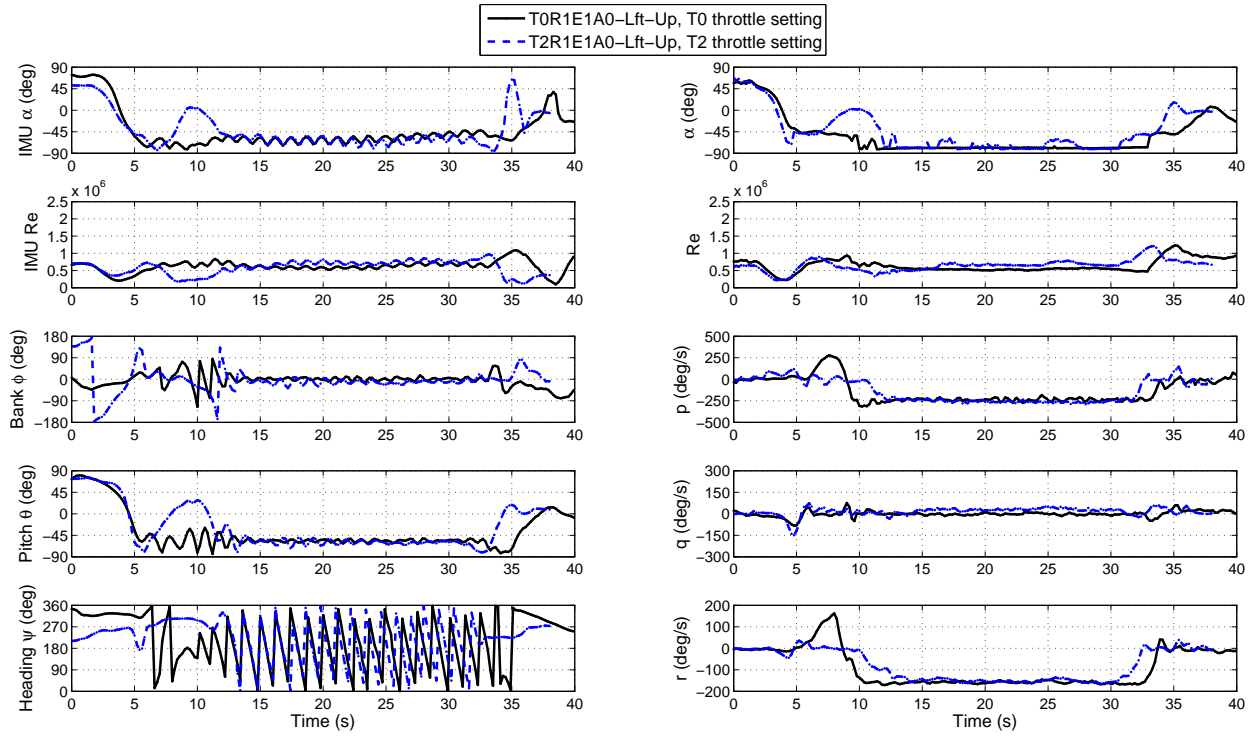


Figure 21. T0R1E1A0-Lft-Up and T2R1E1A0-Lft-Up spins performed on the same flight (effect of throttle setting).

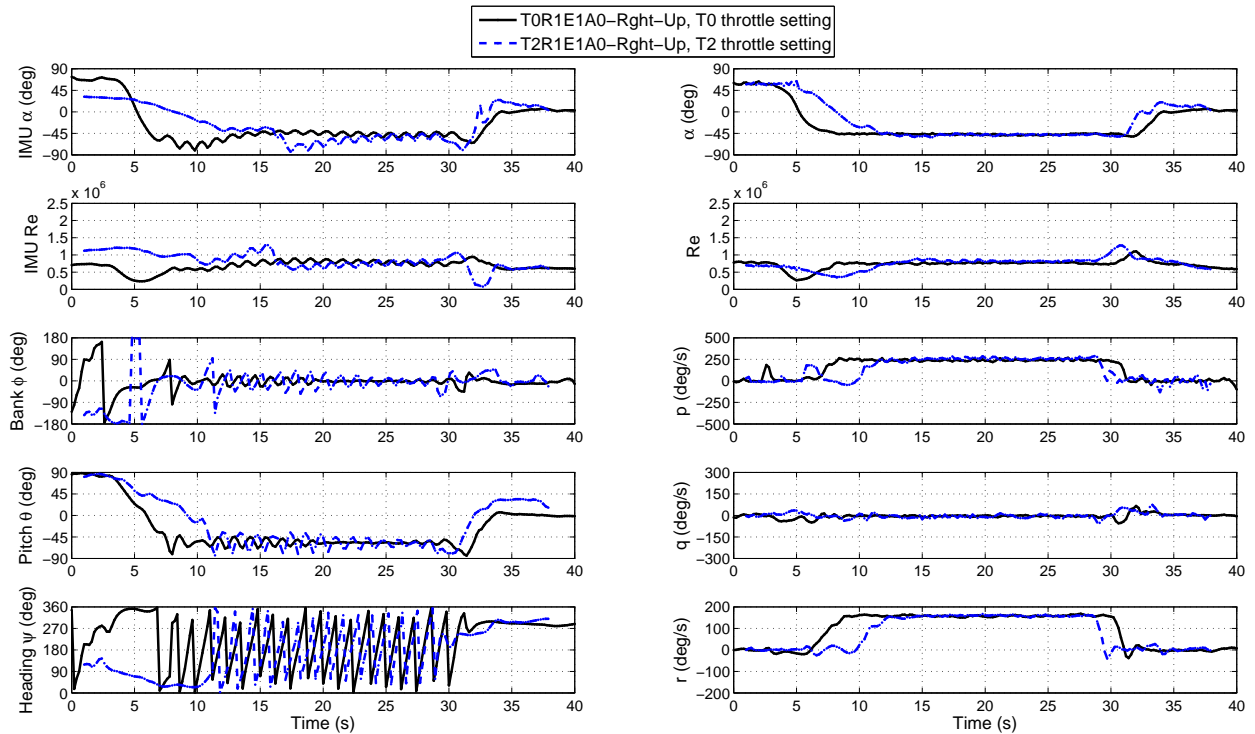


Figure 22. T0R1E1A0-Rght-Up and T2R1E1A0-Rght-Up spins performed on the same flight (effect of throttle setting).

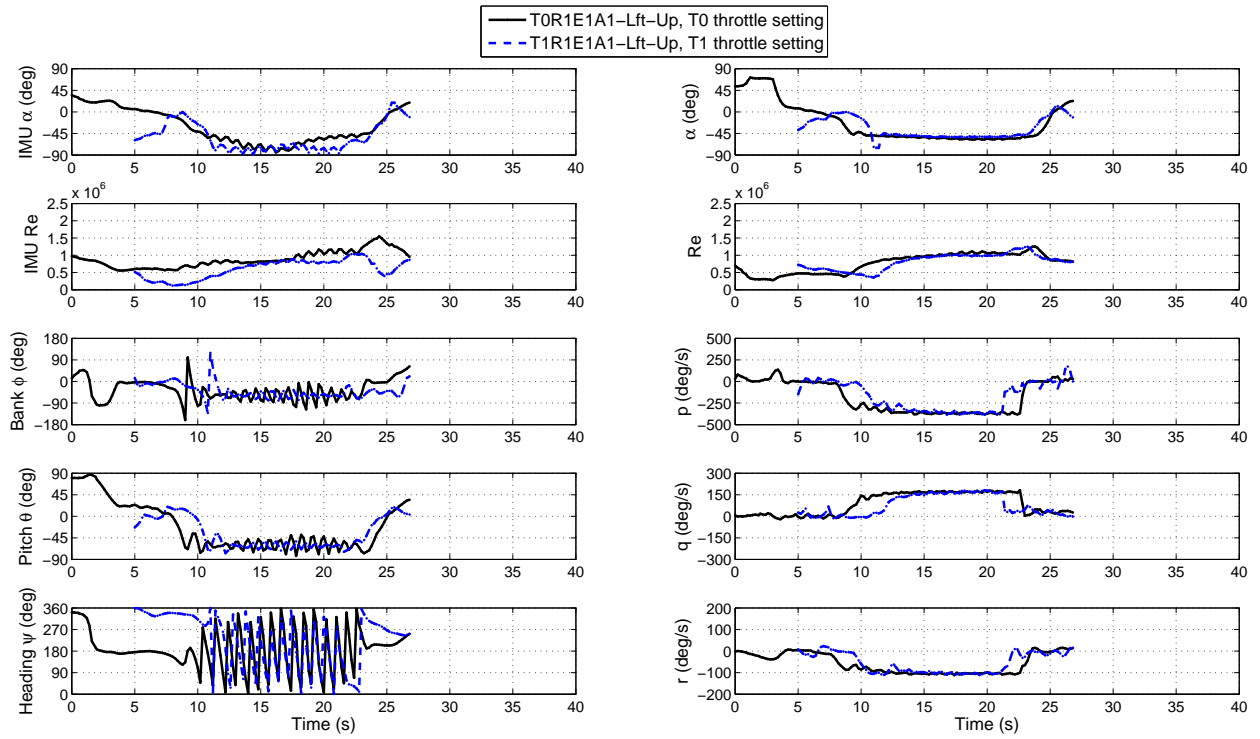


Figure 23. T0R1E1A1-Lft-Up and T1R1E1A1-Lft-Up spins performed on the same flight (effect of throttle setting with pro-spin ailerons).

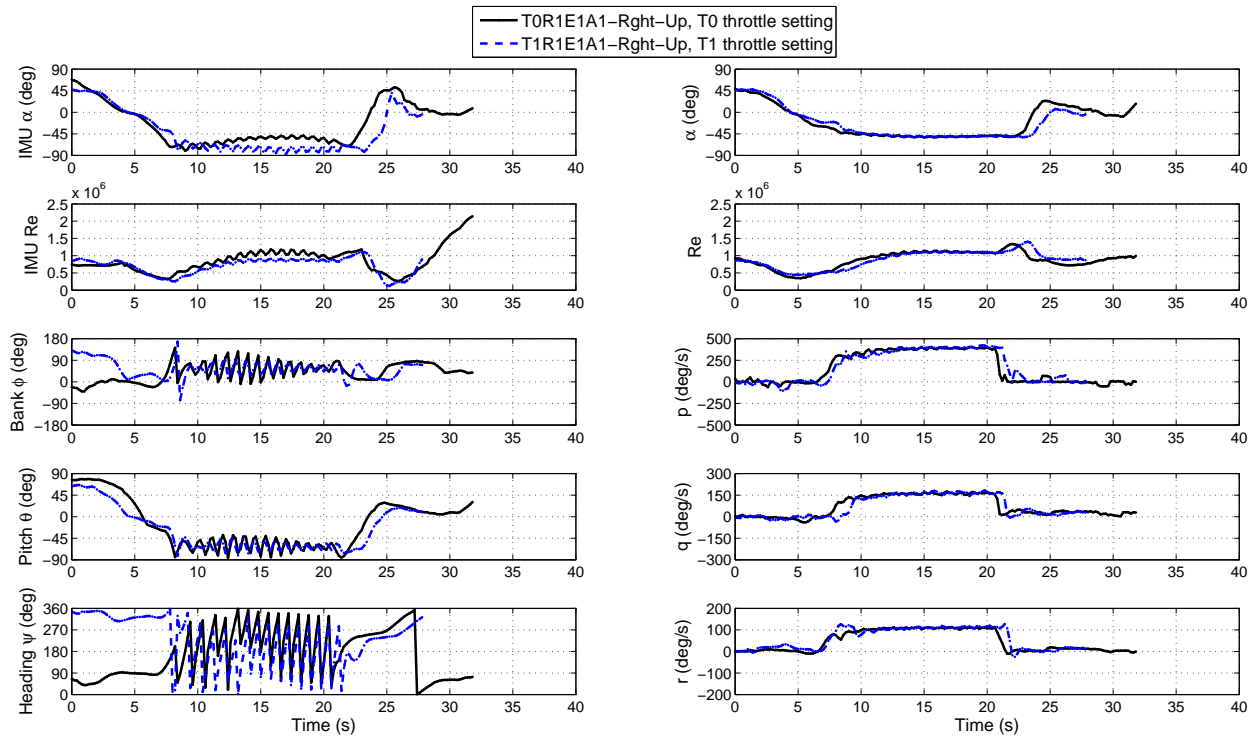


Figure 24. T0R1E1A1-Rght-Up and T1R1E1A1-Rght-Up spins performed on the same flight (effect of throttle setting with pro-spin ailerons).

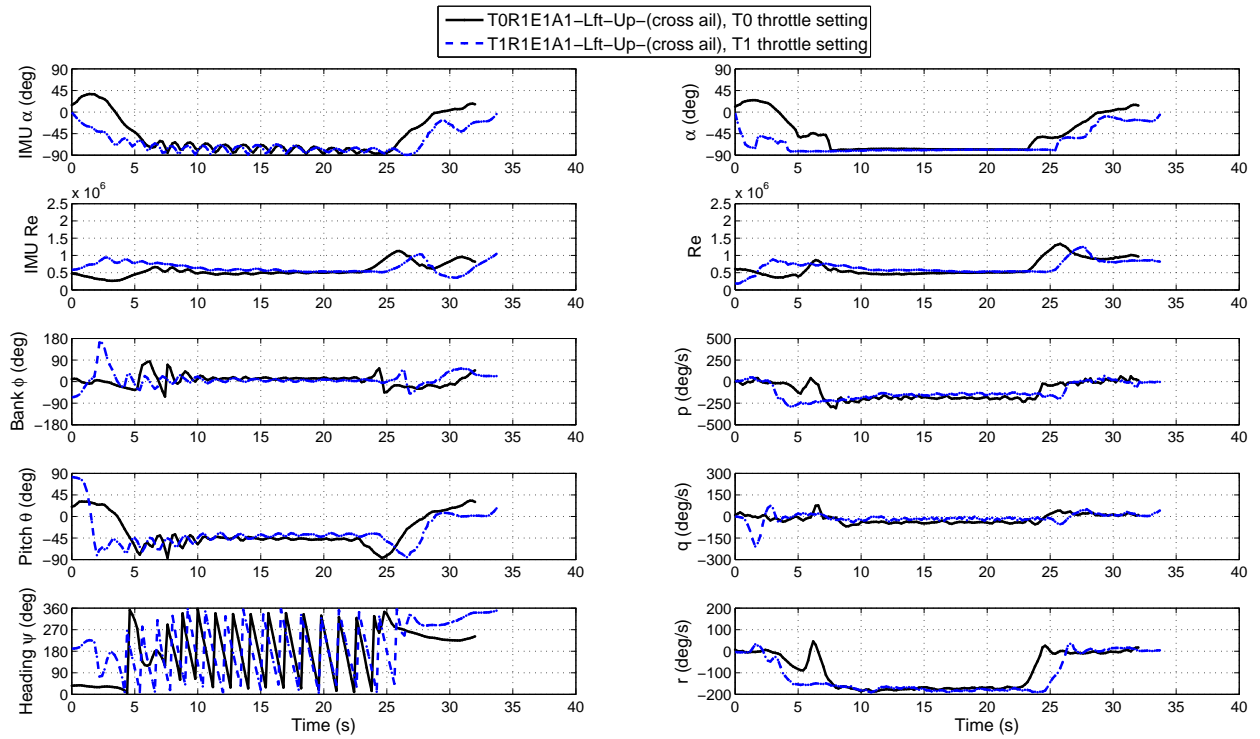


Figure 25. T0R1E1A1-Lft-Up-(cross ail) and T1R1E1A1-Lft-Up-(cross ail) spins performed on two different days (effect of throttle setting with anti-spin ailerons).

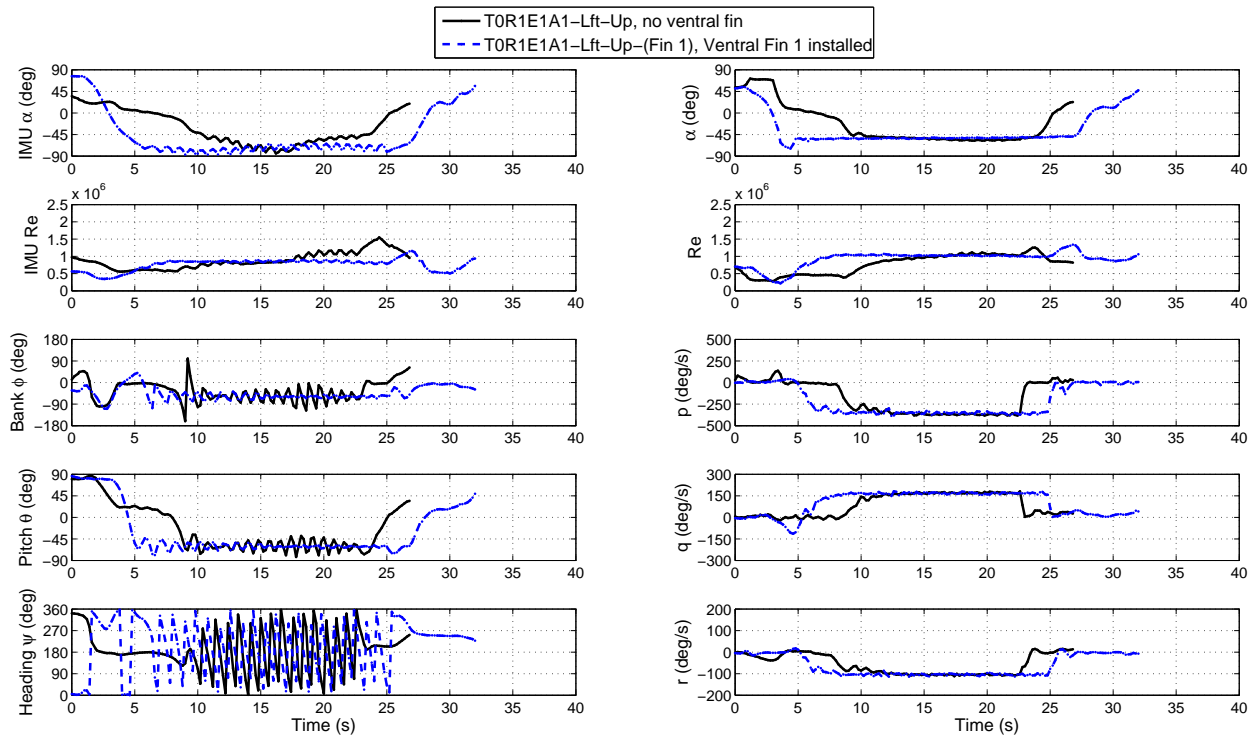


Figure 26. T0R1E1A1-Lft-Up and T0R1E1A1-Lft-Up-(Fin 1) spins performed on two different days (effect of Ventral Fin 1).

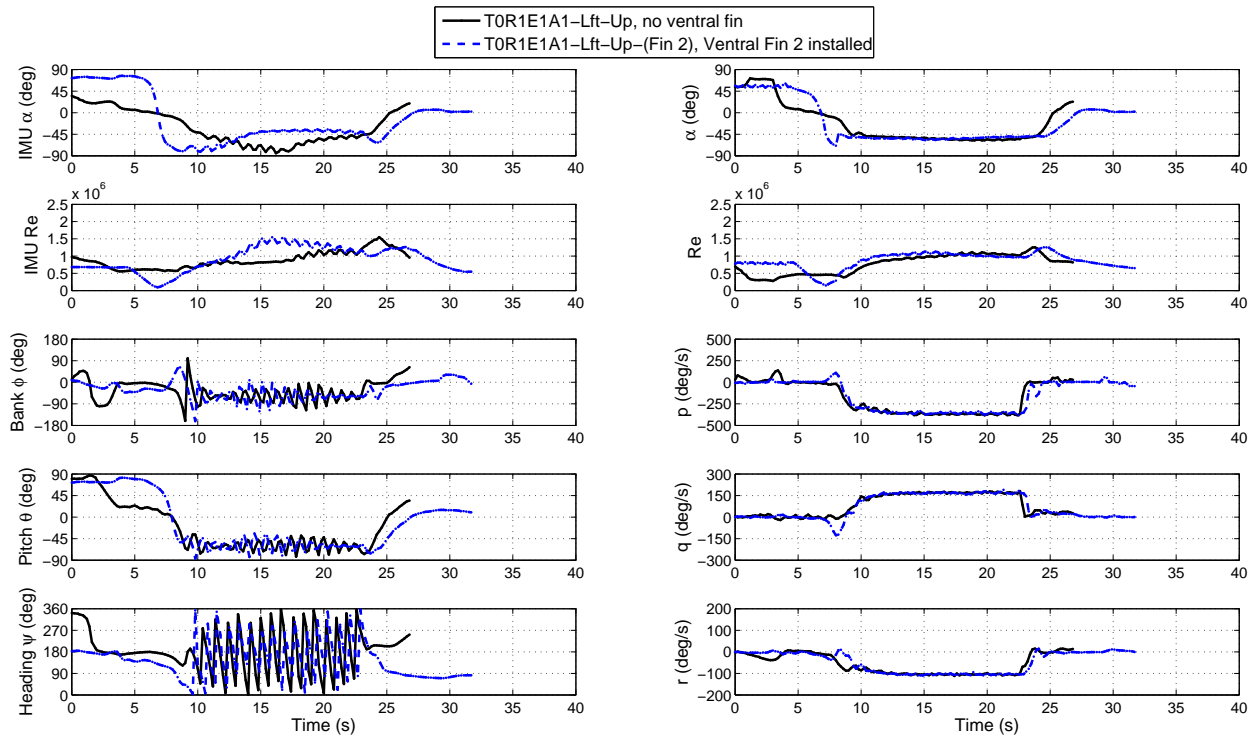


Figure 27. T0R1E1A1-Lft-Up and T0R1E1A1-Lft-Up-(Fin 2) spins performed on two different days (effect of Ventral Fin 2).

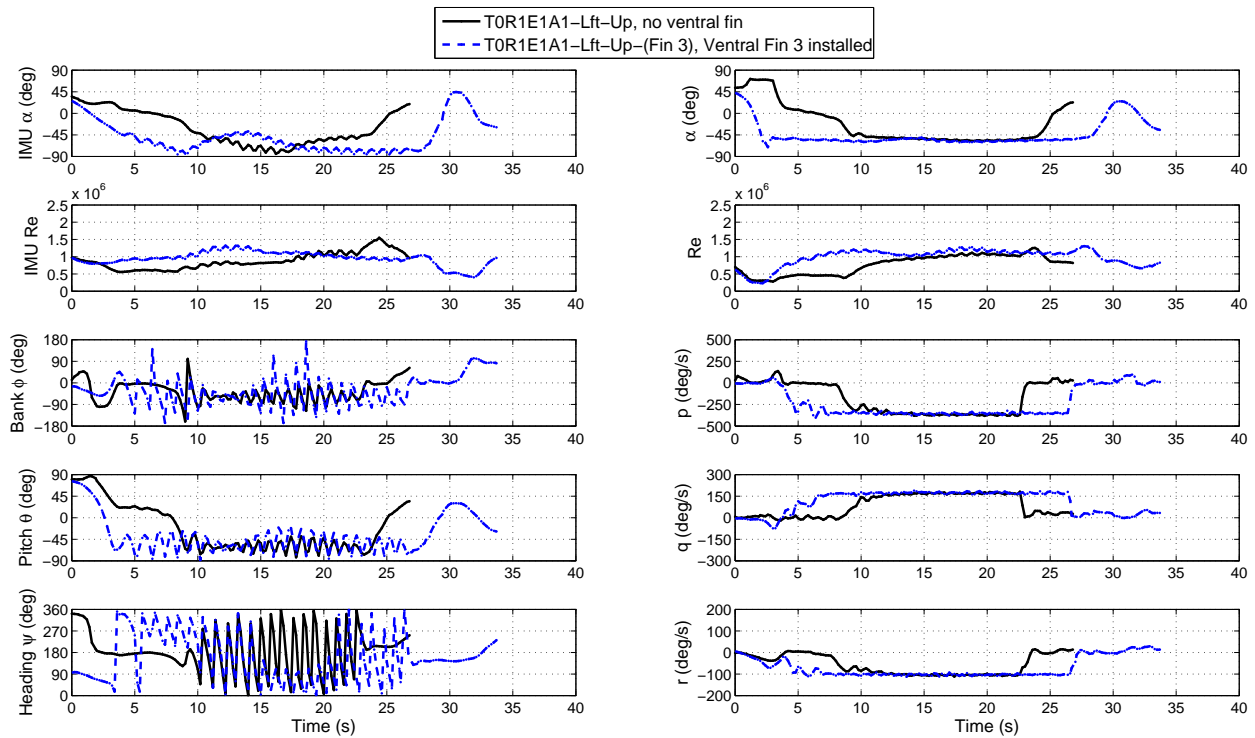


Figure 28. T0R1E1A1-Lft-Up and T0R1E1A1-Lft-Up-(Fin 3) spins performed on two different days (effect of Ventral Fin 3).

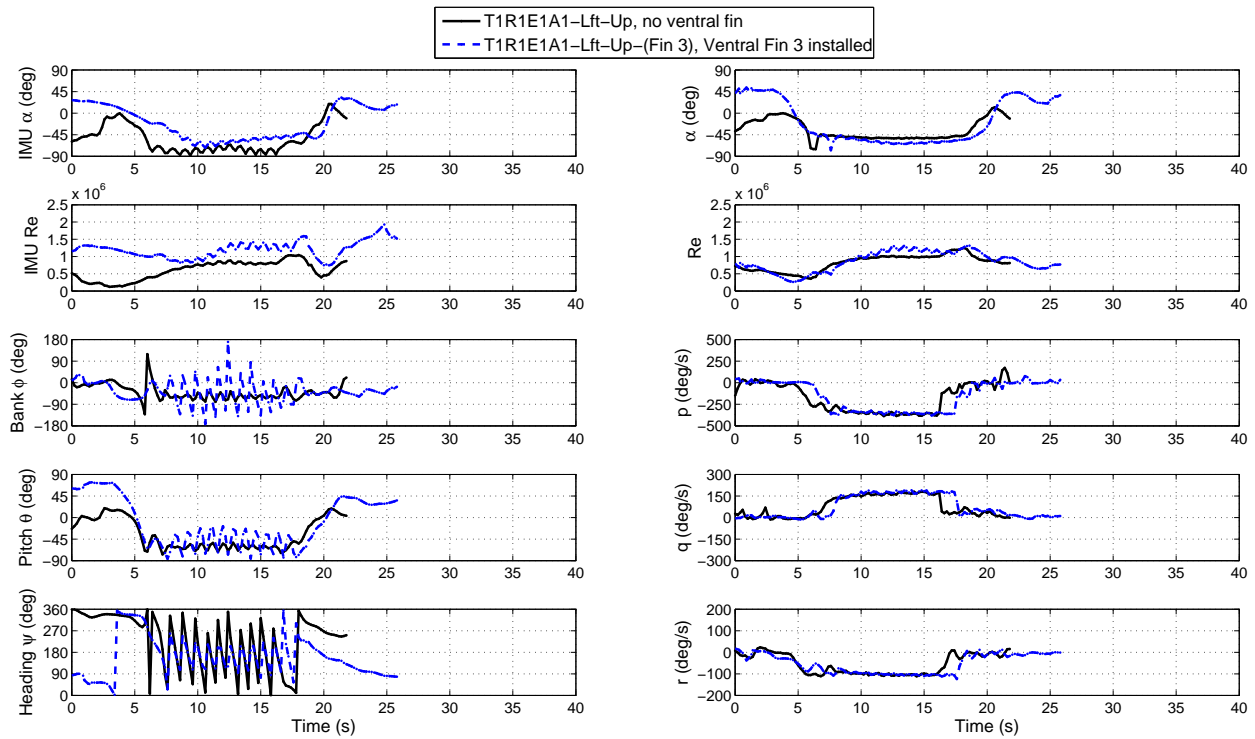


Figure 29. T1R1E1A1-Lft-Up and T1R1E1A1-Lft-Up-(Fin 3) spins performed on two different days (effect of Ventral Fin 3 with non-zero throttle).

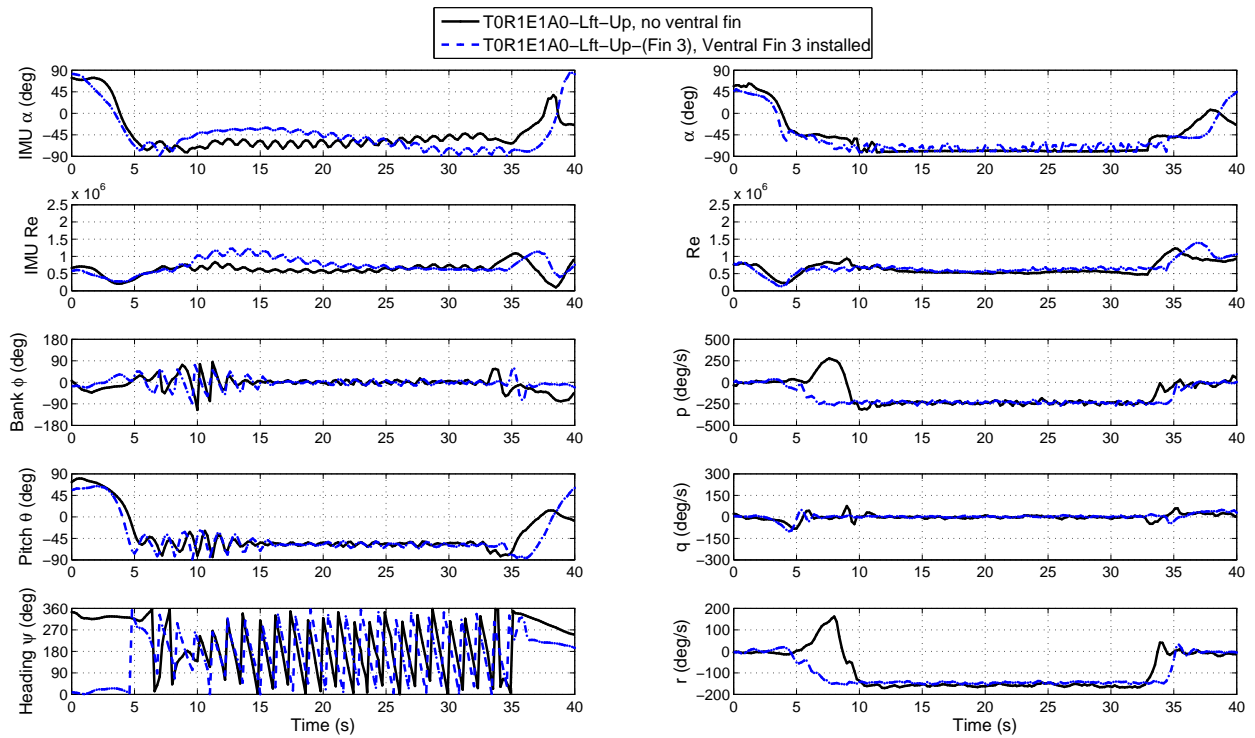


Figure 30. T0R1E1A0-Lft-Up and T0R1E1A0-Lft-Up-(Fin 3) spins performed on two different days (effect of Ventral Fin 3 with neutral ailerons).

## References

- <sup>1</sup>Zimmerman, C. H., "Preliminary Tests in the NACA Free-Spinning Wind Tunnel," NACA Report 557, 1937.
- <sup>2</sup>Soule, H. A. and Scudder, N. F., "A Method of Flight Measurement of Spins," NACA Report 377, 1931.
- <sup>3</sup>Stephens, A. V., "Recent Research on Spinning," *Royal Aircraft Society Journal*, November 1933, pp. 944–955.
- <sup>4</sup>Hreha, M. A. and Lutze, F. H., "A Dynamic Model for Aircraft Poststall Departure," AIAA Paper 83-0367, 1983.
- <sup>5</sup>Lutze, F. H. and Lluch, D., "Simulation of Stall, Spin, and Recovery of a General Aviation Aircraft," AIAA Paper 96-3409, 1996.
- <sup>6</sup>Feistel, T. W. and Anderson, S. B., "Alleviation of Spin-Entry Tendencies through Localization of Wing-Flow Separation," *Journal of Aircraft*, Vol. 18, No. 2, 1981, pp 69–75.
- <sup>7</sup>Pamadi, B. N. and Taylor, L. W., "Estimation of Aerodynamic Forces and Moments on a Steadily Spinning Airplane," *Journal of Aircraft*, Vol. 21, No. 12, 1984.
- <sup>8</sup>Polhamus, E. C., "Effect of Flow Incidence and Reynolds Number on Low-Speed Aerodynamic Characteristics of Several Noncircular Cylinders with Applications to Directional Stability and Spinning," NASA TN 4156, January 1958.
- <sup>9</sup>Adams, W. M., "Analytic Prediction of Airplane Equilibrium Spin Characteristics," NASA Technical Paper TN D-6926, November 1972.
- <sup>10</sup>AOPA Air Safety Foundation, "Joseph T. Nall Reports (1997-2010)," <http://www.aopa.org/asf/publications/nall.html>, Accessed January 2012.
- <sup>11</sup>Anderson, S. B., "Historical Overview of Stall/Spin Characteristics of General Aviation Aircraft," *Journal of Aircraft*, Vol. 16, No. 7, 1978, pp 455–461.
- <sup>12</sup>"Special Study: General Aviation Stall/Spin Accidents 1967-1969," National Transportation Safety Board NTSB-AAS-72-8, September 1972.
- <sup>13</sup>Neihouse, A. I., Lichtenstein, J. H., and Pepoon, P. W., "Tail-Design Requirements for Satisfactory Spin Recovery," NASA Technical Note TN 1045, April 1946.
- <sup>14</sup>Bowman, J. S., "Summary of Spin Technology as Related to Light General-Aviation Airplanes," NASA TN D-6575, December 1971.
- <sup>15</sup>Burk, S. M., Bowman, J. S., and White, W. L., "Spin-Tunnel Investigation of the Spinning Characteristics of Typical Single-Engine General Aviation Airplane Designs," NASA TP-1009, December 1977.
- <sup>16</sup>Stough, H. P., Patton, J. M., and Sliwa, S. M., "Flight Investigation of the Effect of Tail Configuration on Stall, Spin, and Recovery Characteristics of a Low-Wing General Aviation Research Airplane," NASA Technical Paper TP-2644, February 1987.
- <sup>17</sup>Kimberlin, R. D., *Flight Testing of Fixed-Wing Aircraft*, American Institute of Aeronautics and Astronautics, 2003.
- <sup>18</sup>McCormick, B. W., *Aerodynamics Aeronautics and Flight Mechanics*, John Wiley & Sons, New York, NY, 2nd ed., 1995.
- <sup>19</sup>Chambers, J. R., *Concept to Reality: Contributions of the NASA Langley Research Center to U.S. Civil Aircraft of the 1990s*, NASA History Series, 2003.
- <sup>20</sup>Beaurain, L., "General Study of Light Plane Spin, Aft Fuselage Geometry, Part 1," NASA Technical Translation TTF-17,446, 1977.
- <sup>21</sup>Bihrlé, W. and Bowman, J. S., "Influence of Wing, Fuselage, and Tail Design on Rotational Flow Aerodynamics Beyond Maximum Lift," *Journal of Aircraft*, Vol. 18, No. 11, 1981, pp. 920–925.
- <sup>22</sup>Manfriani, L., "Design for Spin," *Proceedings of the 2006 International Council of the Aeronautical Sciences (ICAS) Conference*, 2006.
- <sup>23</sup>Sobie, B., "Flightglobal Pro - PICTURE: Flight gets first look at redesigned SkyCatcher," <http://www.flightglobal.com/news/articles/picture-flight-gets-first-look-at-redesigned-skycatcher-322034/>, Accessed October 2012.
- <sup>24</sup>Sobie, B., "Flight International - OSHKOSH 2009: PICTURES: VIDEO: Cessna unveils revised SkyCatcher," <http://www.flightglobal.com/news/articles/oshkosh-2009-pictures-video-cessna-unveils-revised-skycatcher-330157/>, Accessed October 2012.
- <sup>25</sup>Dantsker, O. D., Johnson, M. J., Selig, M. S., and Bretl, T. W., "Development of the UIUC Aero Testbed: A Large-Scale Unmanned Electric Aerobatic Aircraft for Aerodynamics Research," AIAA Applied Aerodynamics Conference, San Diego, California, June 2013.
- <sup>26</sup>Hangar 9, "35% Extra 260 ARF: Hangar 9," <http://www.hangar-9.com/products/default.aspx?prodid=han1000>, Accessed March 2012.
- <sup>27</sup>Xsens Technologies B.V., "MTi-G User Manual and Technical Documentation, Rev. G," *Xsens Technologies B.V.*, 2009.
- <sup>28</sup>Eagle Tree Systems, "User Manual for the Seagull Wireless Dashboard Telemetry and Data Recorder Systems: Pro, Flight, Glide, Boat," *Eagle Tree Systems LLC*, Revision 4.3.
- <sup>29</sup>Eleodis Electronic Components Distributor, "Miniature Amplified Pressure Sensors Specification Sheet," *Allsensors.com*, 2012.
- <sup>30</sup>Tischler, M. B. and Barlow, J. B., "Determination of the Spin and Recovery Characteristics of a General Aviation Design," *Journal of Aircraft*, Vol. 18, No. 4, 1981, pp. 238–244.
- <sup>31</sup>Bihrlé, W. and Barnhart, B., "Spin Prediction Techniques," *Journal of Aircraft*, Vol. 20, No. 2, 1983, pp. 97–101, pp. 97–101.
- <sup>32</sup>Pamadi, B. N. and Jr., L. W. T., "Semiempirical Method for Prediction of Aerodynamic Forces and Moments on a Steadily Spinning Light Airplane," AIAA Paper 2009-536, January 2009.
- <sup>33</sup>Seidman, O. and Neihouse, A. I., "Free-Spinning Wind-Tunnel Test of a Low-Wing Monoplane with Systematic Changes in Wings and Tails: V. Effect of Airplane Relative Density," NACA Report 691, 1940.
- <sup>34</sup>"FS One, Precision RC Flight Simulator," Version 2, Software Developed by InertiaSoft, Champaign, IL, 2013.
- <sup>35</sup>Lambert, J. D., *Numerical Methods for Ordinary Differential Systems: The Initial Value Problem*, John Wiley and Sons, 2000.
- <sup>36</sup>14 C.F.R., Part 91, §91.126, "Federal Aviation Regulations / Aeronautical Information Manual (FAR/AIM)," 2013.